Universidade de Aveiro
2014
Departamento de Engenharia de Materiais e Cerâmica

Rui Manuel de Oliveira Pinho

Propriedades electromecânicas de cerâmicos de $K_{0.5}Na_{0.5}NbO_3$ texturizado

Electromechanical properties of textured $K_{0.5}Na_{0.5}NbO_3$ ceramics

Universidade de Aveiro
2014
Departamento de Engenharia de Materiais e Cerâmica

Rui Manuel de Oliveira Pinho

Propriedades electromecânicas de cerâmicos de $K_{0.5}Na_{0.5}NbO_3$ texturizado

Electromechanical properties of textured $K_{0.5}Na_{0.5}NbO_3$ ceramics

Tese apresentada à Universidade de Aveiro para cumprimento dos requisitos necessários à obtenção do grau de Mestre em Engenharia de Materiais, realizada sob a orientação científica da Doutora Paula M. L. S. Vilarinho, Professora Associada do Departamento de Engenharia de Materiais e Cerâmica da Universidade de Aveiro e da Doutora Maria Elisabete J. V. Costa, Professora Auxiliar do Departamento de Materiais e Cerâmica da Universidade de Aveiro.

Thesis presented to the University of Aveiro in fulfillment of the requirement for the awarding of the degree of Master in Materials Engineering, under the scientific guidance of Professor Paula M. L. S. Vilarinho, Associated Professor of the Department of Materials and Ceramics Engineering of the University of Aveiro and Professor Maria Elisabete J. V. Costa, Auxiliar Professor of the Department of Materials and Ceramics Engineering of the University of Aveiro.

o júri

presidente

Prof. Doutor Pedro Manuel Lima de Quintanilha Mantas
Professor Auxiliar da Universidade de Aveiro

Prof. Doutor Luís Manuel Cadillon Martins Costa
Professor Associado com Agregação da Universidade de Aveiro

Prof. Doutora Paula Maria Lousada Silveirinha Vilarinho
Professora Associada da Universidade de Aveiro

agradecimentos

I am mostly grateful to my supervisors Prof. Paula M. Vilarinho and Prof. M. Elisabete V. Costa for their support, wisdom and guidance during this work.

I would like to thank the staff members of the department: Maria João Bastos, Ana Ribeiro, Célia Miranda, Marta Ferro, Bruno Almeida, Jacinto Alves, Octávio Contente and Luísa Costa for their effort and sympathy.

I am very grateful to all my colleagues: Sebastian Zlotnik, Pedro Duarte, Pedro Marques, Manuela Fernandes, Cátia Ferreira, Monika Tomczyk, Amit Mahajan, Nathalie Barroca, Alícia Alves, Priscila Melo and Mariza Costa for their positive attitude, friendly working environment and for their skills and knowledge which help me in difficult times.

I would like to thank to Muhammad Asif Rafiq for his time, patience and his kind guidance during this work.

I am also very grateful to all my friends who have listened, supported and gave me strength in hard times. To all of them: thank you!

Por fim, gostaria de agradecer aos meus pais por todo o suporte e confiança depositados em mim ao longo de todos estes anos. Definitivamente sem eles não seria possível para mim apresentar este trabalho hoje. Muito obrigado por tudo.

Rui Manuel de Oliveira Pinho
Aveiro, Portugal

palavras-chave

Niobato de potássio e sódio, $K_{0.5}Na_{0.5}NbO_3$, KNN, materiais isentos de chumbo, cerâmicos policristalinos, cerâmicos texturizados, microestrutura, propriedades dieléctricas e piezoeléctricas.

resumo

Este trabalho é acerca de materiais cerâmicos isentos de chumbo destinados a aplicações electromecânicas e candidatos à substituição de electrocerâmicos à base de chumbo.

O titanato zirconato de chumbo (PZT) é o cerâmico piezoeléctrico mais utilizado em todo o mundo. No entanto, contém mais de 60 wt% de chumbo que é um elemento tóxico para os seres humanos e para o ambiente. Em 2003, a União Europeia aprovou uma directiva proibindo e restringindo o uso de elementos potencialmente perigosos como o chumbo. Devido à inexistência de materiais aptos para a substituição do PZT, foi feita uma exceção até ser encontrado um material alternativo competitivo.

O niobato de potássio e sódio ($K_{0.5}Na_{0.5}NbO_3$, KNN), devido à sua elevada temperatura Curie e propriedades piezoeléctricas moderadas, é um dos materiais isentos de chumbo mais promissores para substituição do PZT. No entanto, a sua efetiva adopção industrial requer, entre outros aspectos, a optimização das suas propriedades.

Neste contexto, estudou-se neste trabalho o efeito de dopantes, da temperatura de sinterização e da texturização em cerâmicos de KNN. Foram fabricados cerâmicos de KNN dopados com i) 1,5 mol% CuO + 2,0 mol% Li_2O, ii) 1,5 mol%CuO + 4,0 mol% Li_2O e iii) 1,5 mol% CuO + 0,5 mol% MnO e sinterizados a diferentes temperaturas (1050, 1065 e 1080 ºC). Complementarmente com o objectivo de maximizar a orientação cristalográfica preferencial dos cerâmicos de KNN (texturização), neste caso segundo a direcção (h00), foram produzidos monocristais de KNN. Estes cristais foram usados como sementes no processo de texturização de cerâmicos de KNN.

Verificou-se que a composição dopada com cobre e manganês foi a única das composições estudadas que se apresentou monofásica. Foram conseguidos cerâmicos, texturizados e não texturizados, densos (> 95 %) e com factor de Lotgering mais elevado dentre as composições estudadas (≈ 20 %). Foi possível demonstrar a dependência das propriedades dieléctricas do factor de Lotgering.

Na tentativa de optimizar o factor de Lotgering para majorar as propriedades piezoeléctricas, foi estudado, para a composição dopada com cobre e manganês, o efeito da quantidade de monocristais adicionada, da taxa de aquecimento e arrefecimento e da duração do patamar de sinterização. Para tal, foram processados cerâmicos de KNN texturizados e dopados com 1,5 mol% de CuO e 0,5 mol% MnO, usando 2,5 wt%, 5,0 wt% e 10,0 wt% de monocristais. Para a mesma composição foi variada a taxa de aquecimento entre 2 ºC/min e 20 ºC/min e o patamar de sinterização entre 4 e 24 h.

Foram conseguidos cerâmicos densos e monofásicos e um incremento no factor de Lotgering de ≈20 % para ≈38 %, para cerâmicos de KNN dopados com 1.5 mol % de cobre e 0.5 mol % de manganês, texturizados com 5 wt% de monocristais e sinterizados a 1065 ºC por 24 h com uma taxa de aquecimento / arrefecimento de 10 ºC/min.

Estes cerâmicos exibem uma permitividade relativa de ≈ 300 à temperatura ambiente, para um valor da temperatura de Curie que se manteve elevado (TC ≈ 400 ºC).

O coeficiente piezoeléctrico aumentou (d_{33} = 65 pC/N) com o aumento de texturização. Apesar do valor do coeficiente piezoelétrico conseguido ser ainda modesto, a constante de voltagem piezoeléctrica destes cerâmicos revelou valores (g_{33} = 23.9*10^{-3} Vm/N) comparáveis com os valores apresentados por certas composições de PZT comercial, mostrando claramente oportunidades competitivas em aplicações (nomeadamente como sensores piezoeléctricos) de cerâmicos de KNN.

Os resultados obtidos neste trabalho contribuem para o conhecimento na área dos materiais piezoeléctricos isentos de chumbo.

keywords

Potassium sodium niobate, $K_{0.5}Na_{0.5}NbO_3$, KNN, lead free materials, polycrystalline ceramics, microstructure, textured ceramics, dielectric and piezoelectric properties.

abstract

This work is about lead-free ceramic materials intended for electromechanical applications and candidates to replace lead-based electroceramics.

One of the most widely used piezoelectric ceramics is lead zirconate titanate (PZT). However, it contains more than 60% of lead and it is toxic for humans and environment. In 2003, a directive from European Union has prohibited the use of potentially hazardous elements as lead. Due to the lack of competitive materials for PZT replacement an exception was created until a competitive alternative be found.

Potassium and sodium niobate due to its high Curie temperature and moderate piezoelectric properties is currently one of the most promising lead-free materials for PZT substitution. However, its effective industrial adoption requires, among others, optimization of its properties.

In this context, in this work we initially studied the effect of dopants, texturing and sintering temperature of KNN ceramics.

For this purpose KNN ceramics doped with i) 1.5 mol% CuO + 2.0 mol% Li_2O, ii) 1.5 mol% CuO + 4.0 mol% Li_2O and iii) 1.5 mol% CuO + 0.5 mol% MnO using different sintering temperatures (1050, 1065 and 1080 °C) were prepared. In addition in order to maximize the preferential crystallographic orientation of the ceramic KNN (texturing), in this case in the direction (h00), KNN single crystals were produced. These crystals were used as seeds in the texturing process KNN ceramics.

It was found that the composition doped with copper and manganese was the only single phase one of the studied compositions. Dense (> 95%) ceramics, textured and non-textured, and with a high Lotgering factor among the studied compositions (≈ 20%) were prepared. The dependence of the dielectric properties of the Lotgering factor was demonstrated.

In the attempt to optimize the Lotgering factor to top up the piezoelectric properties, the effect of the quantity of added crystals, heating and cooling rate and duration of sintering cycle were studied for the composition doped with copper and manganese. To this end, KNN textured ceramics and doped with 1.5 mol% of CuO and 0.5 mol% MnO, using 2.5, 5.0 and 10.0 wt% of single crystals were processed. For the same composition the heating rate of 2 °C/min and 20 °C/min and sintering level between 4 and 24 h was varied.

Dense single phase KNN ceramics with an increase in the Lotgering factor from ≈20% to ≈38% for KNN ceramics doped with 1.5 mol% of copper and 0.5 mol% of manganese, textured with 5 wt% crystals and sintered at 1065 °C for 24 h with a heating rate/cooling of 10 °C/min have been achieved. These ceramics exhibit a relative permittivity at room temperature ≈ 300 for a Curie temperature value which remained high (TC ≈ 400 °C).

The piezoelectric coefficient increased (d_{33} = 65 pC/N) with increased texturing. Despite the value of the piezoelectric coefficient achieved is still modest, the obtained piezoelectric voltage constant revealed values (g_{33} = 23.9 * 10^{-3} Vm/N) comparable to the values reported for certain compositions of commercial PZT, showing clearly competitive opportunities in applications (such as piezoelectric sensors) for KNN ceramics.

The results of this study definitely contribute to the knowledge in the field of lead-free piezoelectric materials.

Table of Contents

Introduction 1

Motivation 1
Objectives 2
State of the Art 3

Dielectric ceramics 3
Piezoelectric ceramics 4
Pyroelectric ceramics 6
Ferroelectric ceramics 6
Potassium Sodium Niobate 8
Template grain growth (TGG) 13
Experimental 15

Polycrystalline KNN ceramics 16
KNN single crystals 17
Textured KNN ceramics 18
Sintering conditions 19
Experimental techniques 19
X-Ray diffraction (XRD) 19
Scanning electron microscopy (SEM) 20
Dielectric measurements 20
Piezoelectric coefficient 22
Results and Discussion 23

Part I 23
Abstract 23
KNN single crystals and powder characterization 23
Untextured doped KNN ceramics 29
Textured doped KNN ceramics 34
Discussion 43
Part II 45
Abstract 45
Phase purity 45
Degree of texture 47
Microstructure and density of sintered samples 47
Dielectric properties 50

Piezoelectric properties 54
Discussion 56
Conclusions 59
References 61

List of Figures

Figure 1 - Illustration of the piezoelectric effect (direct and converse effects) [8]. 4
Figure 2 - Illustration of the forces that influence a piezoelectric element [10]. 5
Figure 3 - Perovskite ABO_3 unit cell [9]. 7
Figure 4 - Schematic representation of the poling process of a piezoelectric ceramic; on the left random orientation of polar domains, in the center polar domains ordered along the DC electric field and on the right polar domains after the electric field has been removed, corresponding to a remnant polarization [10]. 8
Figure 5 - Relation between di-, piezo-, pyro- and ferroelectrics. 8
Figure 6 - Dielectric permittivity and piezoelectric coefficient vs. Curie temperature for various polycrystalline piezoelectrics [13]. 9
Figure 7 - Phase diagram of KNbO3-NaNbO3 system [13]. 10
Figure 8 - Flowchart of the work carried out in this work. 15
Figure 9 - Schematic representation of the furnace and crucible positions used for the growth KNN single crystals. 17
Figure 10 - Thermal profile used for the growth of KNN single crystals. 18
Figure 11 - Equivalent circuit diagrams of capacitive cell (a) of charging and loss current (b) and of loss tangent for a typical dielectric (c) [22]. 21
Figure 12 - Schematic representation of the Berlincourt. 22
Figure 13 - X-ray diffraction of KNN single crystals used for texturing and crystallographic planes from the PDF card 00-061-0315. 24
Figure 14 - Photograph of KNN single crystals inside de platinum crucible (left) and KNN single crystals after removing from of the platinum crucible (right). 24
Figure 15 - SEM micrograph of crushed KNN single crystals after sieving. 25
Figure 16 - X-ray diffraction patterns of doped and undoped KNN powders after calcination. 26
Figure 17 - SEM micrographs of KNN powders; a) KNN, b) KNN + 1.5 % CuO + 2 % Li_2O, c) KNN + 1.5 % CuO + 4 % Li_2O, d) KNN + 1.5 % CuO + 0.5 % MnO. 27
Figure 18 - Particle size distribution of KNN powders (doped and undoped). 28
Figure 19 - Dilatometry curves for pure and doped KNN. 29
Figure 20 - X-ray diffraction patterns of the samples of KNN+1.5% CuO+2% Li2O sintered at different temperatures. 30

Figure 21 - X-ray diffraction patterns of the samples of KNN+1.5% CuO+4% Li_2O sintered at different temperatures.....30
Figure 22 - X-ray diffraction patterns of the samples of KNN+1.5% CuO+0.5% MnO sintered at different temperatures.....31
Figure 23 - Relative densities of doped KNN ceramics sintered at different temperatures. 32
Figure 24 - SEM micrographs of doped KNN sintered at different temperatures.....33
Figure 25 - Grain size distribution of doped KNN for different temperatures. 34
Figure 26 - X-ray diffraction patterns of the samples of textured KNN+1.5% CuO+2% Li_2O sintered at different temperatures.....35
Figure 27 - X-ray diffraction patterns of the samples of textured KNN+1.5% CuO+4% Li_2O sintered at different temperatures.....36
Figure 28 - X-ray diffraction patterns of the samples of textured KNN+1.5% CuO+0.5% MnO sintered at different temperatures. 36
Figure 29 - Lotgering factor (%) for textured doped KNN sintered at different temperatures.....37
Figure 30 - Relative densities of textured doped KNN for different sintering temperatures. 38
Figure 31 - SEM micrographs of textured doped KNN sintered at different temperatures. 39
Figure 32 - Grain size distribution of textured samples of doped KNN for different temperatures.....40
Figure 33 - Relative permittivity as a function of temperature for 1kHz of textured doped and untextured undoped KNN ceramics sintered at 1065 ˚C for 2 h.....41
Figure 34 - Dielectric losses as a function of temperature for 1kHz of textured doped and untextured undoped KNN ceramics sintered at 1065 ˚C for 2 h.....42
Figure 35 - X-ray diffraction patterns of the samples of KNN+1.5% CuO+0.5% MnO sintered at 1065 ˚C for 24 hours, ranging the amount of single crystals. 46
Figure 36 - X-ray diffraction patterns of the samples of KNN+1.5% CuO+0.5% MnO sintered at 1065 ˚C for 24 hours, with 5 wt% of single crystals, ranging the heating/cooling rate.....46
Figure 37 - X-ray diffraction patterns of the samples of KNN+1.5% CuO+0.5% MnO sintered at 1065 ˚C with 5 % of single crystals and an heating ratio of 10 ˚C/min, ranging the dwelling time.....47

Figure 38 - SEM micrographs of textured KNN + 1.5 mol% CuO + 0.5 mol% MnO sintered with 10 ˚C/min for 24 h at 1065 ˚C, ranging the amount of single crystals. 49
Figure 39 - SEM micrographs of textured KNN + 1.5 mol% CuO + 0.5 mol% MnO with 5 wt% of single crystals, sintered for 24 h at 1065 ˚C, ranging the heating rate. 50
Figure 40 - SEM micrographs of textured KNN + 1.5 mol% CuO + 0.5 mol% MnO with 5 wt% of single crystals, sintered with 10 ˚C/min at 1065 ˚C, ranging the dwelling time. 50
Figure 41 - Relative permittivity (at 1 kHz) of KNN + 1.5 mol% CuO + 0.5 mol% MnO with 5 wt% of KNN single crystals and sintered at 1065 ˚C with an heating ratio of 10 ˚C/min for different dwell times. 51
Figure 42 - Dielectric losses (at 1 kHz) of KNN + 1.5 mol% CuO + 0.5 mol% MnO with 5 wt% of KNN single crystals and sintered at 1065 ˚C with an heating ratio of 10 ˚C/min for different dwell times.....52
Figure 43 - Magnification of area around O-T transition of KNN + 1.5 mol% CuO + 0.5 mol% MnO with 5% of single crystals sintered at 1065 ˚C for 4, 16 and 24 h with 10 ˚C/min of heating rate and pure KNN sintered at 1100 ˚C for 4 h. 52
Figure 44 - Dielectric permittivity of KNN + 1.5 mol% CuO + 0.5 mol% MnO with 5% of single crystals sintered at 1065 ˚C for 24 h with 10 ˚C/min of heating rate as function of temperature for different frequencies. 53
Figure 45 - Dielectric losses of KNN + 1.5 mol% CuO + 0.5 mol% MnO with 5% of single crystals sintered at 1065 ˚C for 24 h with 10 ˚C/min of heating rate as function of temperature for different frequencies.....54
Figure 46 - Piezoelectric coefficient versus dwell time of KNN + 1.5 mol% CuO + 0.5 mol% MnO with 5% of single crystals sintered at 1065 ˚C with 10 ˚C/min of heating rate. 55
Figure 47 - Piezoelectric voltage constant versus dwell time of KNN + 1.5 mol% CuO + 0.5 mol% MnO with 5% of single crystals sintered at 1065 ˚C with 10 ˚C/min of heating rate.....55

List of Tables

Table 1 - Dielectric permittivity and piezoelectric coefficient (*d33*) for polycrystalline KNN, KNN single crystals, doped KNN and doped/textured KNN ceramics. 12
Table 2 - KNN compositions under study. 16
Table 3 - Raw materials used for preparation of KNN bulk ceramics and single crystals. 16
Table 4 - Curie temperature and relative permittivity for untextured undoped and textured doped KNN samples sintered at 1065 ˚C for 2 h. 42
Table 5 - Calculated Lotgering factors for textured KNN+1.5% CuO+0.5% MnO ceramics. 48
Table 6 - The density of textured KNN + 1.5 mol% CuO + 0.5 mol% MnO ceramics sintered under different conditions. 49
Table 7 - Properties of KNN + 1.5 mol% CuO + 0.5 mol% MnO with 5% of single crystals sintered at 1065 ˚C with 10 ˚C/min of heating rate, ranging the dwelling time (4, 16 and 24 h). 57
Table 8 - Comparison between properties of commercial PZT and KNN + 1.5 mol% CuO + 0.5 mol% MnO with 5% of single crystals sintered at 1065 ˚C with 10 ˚C/min of heating rate, dwelling time (16h). 58

List of Symbols

A - Area

C_p - Capacitance of a parallel plane capacitor

d - Piezoelectric coefficient

d_{33} - Piezoelectric coefficient (induced polarization in direction 3 per unit of stress applied in direction 3)

E - Electrical field

f - Degree of texturing or Lotgering factor

g - Piezoelectric voltage constant

k_{ij} - Electromechanical coupling factor

l - Thickness

M - Molecular weight

P - Electrical polarization

r - radius

R - Gas constant

S - Solubility

T - Temperature

T_C - Curie temperature

$T_{O\text{-}T}$ - Orthorhombic to tetragonal transition temperature

$tan\ \delta$ - Loss tangent

γ - Average surface energy

ε_r - Relative dielectric permittivity

ε_0 - Dielectric permittivity in vacuum

ϵ - Mechanical strain

ρ - Density

σ - Mechanical stress

List of Abbreviations

BT - Barium titanate

EDS - Energy dispersive x-ray spectroscopy

KN - Potassium niobate

KNN - Potassium sodium niobate

NBT - Sodium bismuth titanate

NN - Sodium niobate

PLZT - Lead lanthanum zirconate titanate

PT - Lead titanate

PZT - Lead zirconate titanate

SEM - Scanning electron microscope

TGG - Template grain growth

XRD - X-ray diffraction

Introduction

Motivation

Piezoelectricity was discovered in Rochelle salt, quartz and others minerals by Pierre and Jacques Curie in 1880. Over the years, naturally occurred and synthesized piezoelectrics have been used in several applications such as piezoelectric sonars, ultra-sonic transducers, filters, sensors, inkjet printers and ultrasound imaging equipment.

One of the most widely used piezoelectric ceramics is lead zirconate titanate ($Pb_{1-x}Zr_xTiO_3$, PZT) [1]. However, PZT has more than 60 wt% of lead that is a toxic element to human beings and environment. In 2003, a directive of European Union has prohibited the use of potentially harmful elements, like lead. Due to the inexistence of a proper alternative material suitable to PZT substitution, it was made an exception for PZT till a competitive alternative will be found [2-3]. Therefore, an extensive research on lead free piezoceramics has been promoted. Among the lead free ceramics under investigation, alkali niobates have been described as one the most promising family of compounds [3]. Within this family, potassium sodium niobate ($(K_{0.5}Na_{0.5})NbO_3$ - KNN), due to its high Curie temperature, is a promising lead free piezoelectric and it gained particular importance since the publication of Saito *et al.* in 2004. Saito reported that textured $(K_{0.44}Na_{0.52}Li_{0.04})(Nb_{0.84}Ta_{0.10}Sb_{0.06})$ ceramics exhibit a record d_{33} value of 416 pC/N with T_C of 253 ºC, a value close do the d_{33} of some PZT compositions [4].

However, as Ferroperm Piezoceramics A/S stated in its comments regarding Exemption 7(c): “lead in electronic ceramic parts (e.g. piezoelectronic devices)” [5] a feasible solution for the substitution of PZT has to be economical viable. Therefore, Saito's composition that contains tantalum an expensive rare earth (e.g., Ta_2O_5=1400 €/kg, compared with TiO_2=50 €/kg, PbO=66 €/kg and ZrO_2=220 €/kg [6]) will hardly be a viable commercial alternative for PZT substitution. In order to make KNN economically practicable, much more research and development is necessary to engineer the properties of KNN in order to make them compatible with the electromechanical performance of PZT. Otherwise the implementation of KNN in practical applications will be dependent from political intends.

Objectives

The aim of this work is to contribute to the improvement of the electromechanical properties of potassium sodium niobate ceramics, $(K_{0.5}Na_{0.5})NbO_3$ (KNN), keeping a high Curie temperature (T_C), towards a competitive substitution of lead based $Pb(Zr_xTi_{1-x})O_3$ (PZT). Thus, the microstructure of KNN ceramics was engineered by combining the use of KNN single crystals with selected dopants to achieve preferential crystallographic orientation and maximized density, hence optimized electromechanical properties.

State of the Art

Dielectric ceramics

A material is considered a dielectric when it is characterized by a large electric resistivity. Dielectric materials do not conduct electricity due to its low concentration of free charges. This makes possible their use as insulators. It can be said that all the dielectric materials are insulators but not all the insulators are dielectric materials. A insulator is a material who cannot conduct electricity due to the absence of free electric charges. A dielectric material can be differentiated from an insulator due to its capability to store charge when placed in a capacitor, under an electric field. When an electric field is applied to a dielectric, there is no charges transportation at long distances, only the dislocation of charges centers in small range. The small range charge dislocation forms dipole moments. This phenomenon is known as polarization.

When a dielectric material is placed between two parallel plans of a capacitor, the capacitance increases. The ratio between the values of capacitance with and without material is called the relative dielectric permittivity (ε_r) [7]. The relative dielectric permittivity can be calculated by Equation 1:

$$\varepsilon_r = \frac{C_p l}{\varepsilon_0 A} \qquad \text{Equation 1}$$

where C_p is the capacitor capacitance, l is the thickness of the dielectric, ε_0 is the dielectric permittivity in vacuum (8.85×10^{-12} F/m) and A is the electrode area.

When an electrical field, E, is applied to a dielectric material, it suffers a small change in dimensions. If the resultant strain, ϵ, is proportional to the square of the applied field, the effect is called electrostriction. This effect is described by Equation 2:

$$\epsilon = \xi E^2 \qquad \text{Equation 2}$$

where ξ is the electrostrictive coefficient.

Piezoelectric ceramics

Piezoelectricity was discovered in 1880 in Rochelle salt ($KNaC_4H_4O_6 \cdot 4H_2O$), quartz and other minerals by Jacques and Pierre Curie. Piezoelectricity derives from the Greek *piezo* or *piezein* that means press. Piezoelectricity is a property observed in some materials, consisting on the appearance of an electric polarization when a mechanical stress is applied (direct effect) or a mechanical strain when an electric field is applied (converse effect) [8]. Figure 1 illustrates the piezoelectric effect (direct and converse).

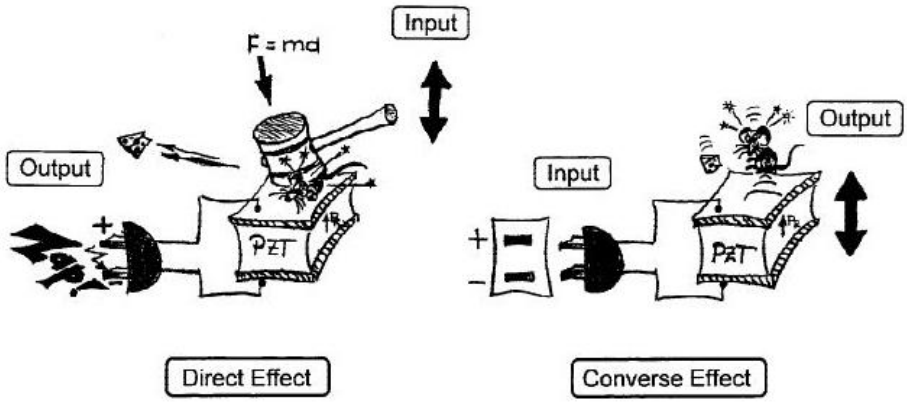

Figure 1 - Illustration of the piezoelectric effect (direct and converse effects) [8].

When a mechanical stress is applied to a piezoelectric, it exhibits a finite polarization value. The resultant polarization is proportional to the applied mechanical stress. This is called direct effect and it is described in Equation 3. When an electrical field is applied to a piezoelectric, it will present a mechanical strain. The resultant mechanical strain is proportional to the applied electrical field. This is called converse effect and it is described in Equation 4.

$$P = d\sigma \ (direct\ effect) \qquad \text{Equation 3}$$

$$\epsilon = dE \ (converse\ effect) \qquad \text{Equation 4}$$

where P is the electrical polarization, d is the piezoelectric coefficient, σ is the mechanical stress, ϵ is the mechanical strain and E is the electrical field. For these two cases, the

piezoelectric coefficient, *d*, is the proportionality between the applied stimulus and the response of the material. The piezoelectric coefficient, *d*, is the same for the direct and converse effects (although with different units) and it is a key coefficient in order to compare piezoelectric response of materials [9]. High *d* materials are often used in sonars or transducers.

The piezoelectric properties are anisotropic so the physical constants implied in piezoelectric effect depend on the direction of the applied stimulus and the measured response. Consequently, the piezoelectric constant has two indices, *i* (*i*= 1, 2, 3) and *j* (*j*= 1, 2, 3, 4, 5, 6), where *i* is the direction of the applied strain or field and *j* is the direction of the measured polarization or mechanical strain. The *j* =1, 2 and 3 are relative to linear response and *j* = 4, 5 and 6 are relative to shear response. Figure 2 shows a schematic illustration of the correlation between these directions.

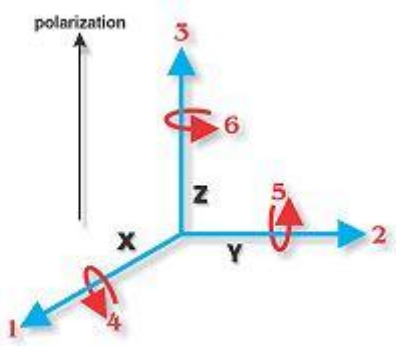

Figure 2 - Illustration of the forces that influence a piezoelectric element [10].

d_{33} is the most reported coefficient for piezoelectric measurements in direct and converse effects. High piezoelectric coefficients materials are usually classified as *soft* ceramics and they are desirable for applications in vibrational devices such as sonars.

Another coefficient used to evaluated piezoelectric ceramics is the piezoelectric voltage constant, *g*. Piezoelectric voltage constant evaluate the ability of a piezoelectric ceramics to generate voltage per unit of input stress or the mechanical strain experienced by a piezoelectric ceramic per unit of electric displacement applied. This constant is related to the piezoelectric coefficient, *d*, by Equation 5.

$$g = \frac{d}{\varepsilon_r \times \varepsilon_0} \qquad \text{Equation 5}$$

where d is the piezoelectric coefficient, ε_r is the relative dielectric constant and ε_0 is the dielectric constant in vacuum. A high g constant is possible for a given d coefficient if the material has a low ε_r. High g constant ceramics are usually classified as *hard* ceramics and they are often used as portable gas igniters [8].

Pyroelectric ceramics

Pyroelectricity was discovered in 1824 in Rochelle Salt. Pyroelectrics are materials that present spontaneous polarization due to its non-symmetric structure. These materials are sensitive to temperature. The spontaneous polarization, P_s, changes when the material is uniformly heated. This effect is described by Equation 6.

$$P_s = pT \qquad \text{Equation 6}$$

where p is the pyroelectric coefficient and T is the temperature.

Ferroelectric ceramics

Sixty years after discovering piezoelectricity, ferroelectricity was reported in Rochelle salt. A material that presents spontaneous polarization and the direction of the polarization is reversible by an electrical field is called ferroelectric. There are only a few crystallographic structures that allow ferroelectricity (tungsten-bronze, perovskite, pyrochlore and bismuth-layer type structures). Among this group of materials, the perovskite one is by far the most important. Belonging to the perovskite group are compositions like $BaTiO_3$ (BT), $Pb_{0.5}Zr_{0.5}TiO_3$ (PZT), $PbTiO_3$ (PT) and $K_{0.5}Na_{0.5}NbO_3$ (KNN).

Perovskite type structures have the compositional form ABO_3, where A and B are cations, normally charged +1, +2 or +3 and +3, +4 or +5 for A and B standing ions, respectively. Figure 3 displays a schematic illustration of a typically perovskite. The A-site ions occupy the vertices of the cube, the B-site ions occupy the center of the cube and the oxygen anions occupy the faces of the cube.

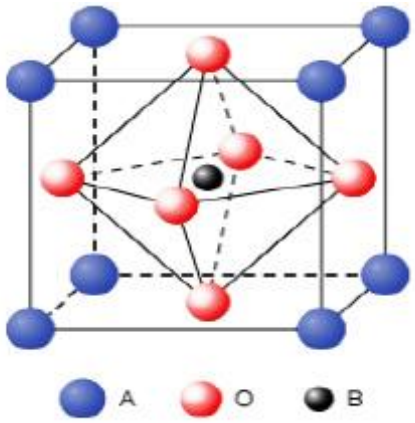

Figure 3 - Perovskite ABO_3 unit cell [9].

In piezoelectrics, pyroelectrics and ferroelectrics, the B-site cation is naturally dislocated from the unit cell center and due to this, all the listed classes present spontaneous polarization. Because the B site cation is dislocated, a dipole is formed. If a group of unit cells present their dipoles aligned in same direction and if this dipoles could be re-oriented to another direction by a high electric field, this area is called ferroelectric domain. In order to allow the transition between two or more dipole directions, the energy difference between them needs to be low. The increasing of the temperature induces the material to transform in a non-polar form. The experimental temperature at which this transition occours is usually called Curie temperature and marks the transition temperature between the ferroelectric state (non center symmetric) to paraelectric state (center symmetric state) [7]. At this point the piezo, pyro and ferroelectric properties are lost until the cooling of the material.

In a polycrystalline ferroelectric ceramic, the ferroelectric domains are randomly oriented, hence, the sum of their contributions to the total polarization is equal to zero. However, when an electric field is applied to a ferroelectric ceramic, all of the B-side cations are dislocated along the electric field direction and a net non zero polarization is created. After the electric field is removed, the B-side cations will remain aligned close to the electric field direction. This process is called polling or piezoelectric activation. Figure 4 presents an illustration of this phenomenon. The original state of randomly oriented domains can be restored by heating the material above its Curie temperature. Above this the ceramic becomes centro-symmetric and losses all the ferroelectric properties. This process is called thermal depolling.

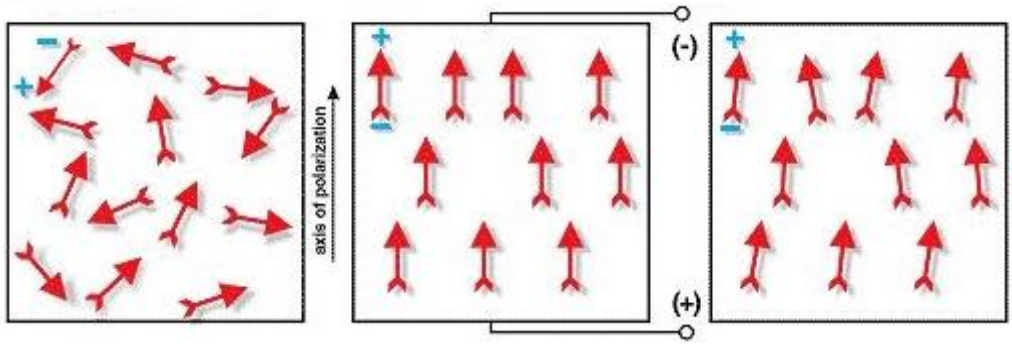

Figure 4 - Schematic representation of the poling process of a piezoelectric ceramic; on the left random orientation of polar domains, in the center polar domains ordered along the DC electric field and on the right polar domains after the electric field has been removed, corresponding to a remnant polarization [10].

The correlations between di-, piezo-, pyro- and ferroelectrics can be illustrated by the schematic representation in Figure 5.

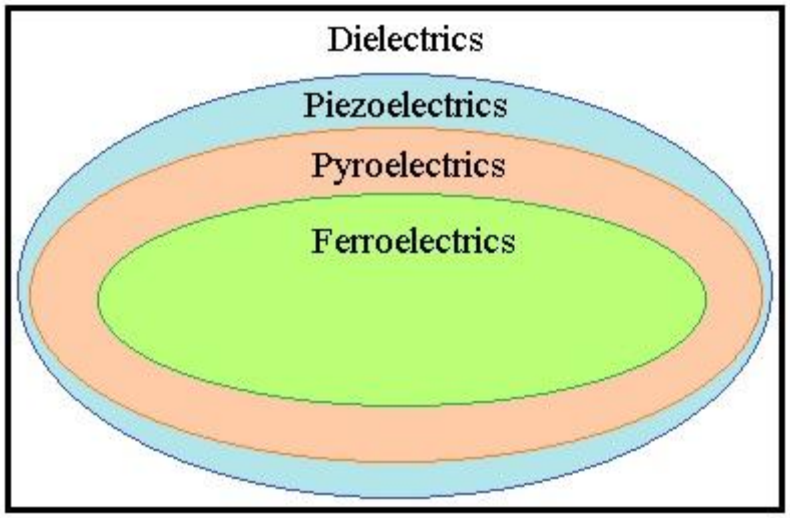

Figure 5 - Relation between di-, piezo-, pyro- and ferroelectrics.

Potassium Sodium Niobate

Since the European Union restricted the use of lead in electronic devices, a raise in the research on lead free piezoelectric has started.

Among lead free piezoelectric ceramics there are three main families, namely $(Na,Bi)TiO_3$ (NBT), BT and KNN. Between them, KNN is considered one of the most

promising lead free system due to its high Curie temperature (T_C = 420 ºC), moderate electrical properties (d_{33} = 80 pC/N, ε_r = 230-475) and possibility of engineering the piezoelectric coefficients by designing the composition and microstructure [11-12]. However, KNN system still needs considerable improvement before it becomes a suitable substitute for PZT (Figure 6).

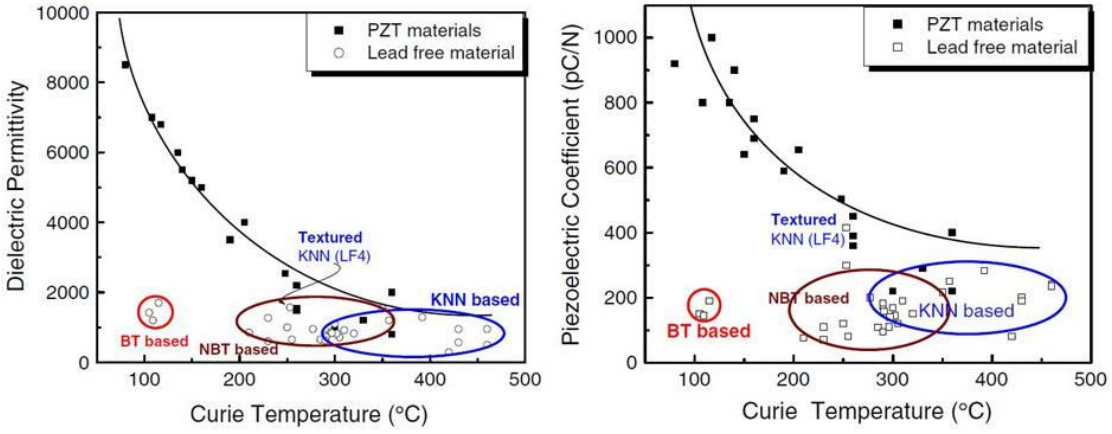

Figure 6 - Dielectric permittivity and piezoelectric coefficient vs. Curie temperature for various polycrystalline piezoelectrics [13].

The lead based materials present better properties than lead free counter parts, however, the lead based materials are limited, by their Curie temperature, for high temperature applications. As can be observed in Figure 6, the dielectric permittivity and piezoelectric coefficient of PZT materials is several times higher when compared with BT and NBT based materials. KNN based materials already presents same compositions with properties in the range of PZT based materials and present moderate values for temperatures at which PZT based materials do not present any values. From this point of view, KNN based materials can be seen as a promising material for high temperature applications.

Potassium sodium niobate is a solid solution of potassium niobate, $KNbO_3$ (KN), and sodium niobate, $NaNbO_3$ (NN). KN and NN are orthorhombic at room temperature.

Figure 7 presents the phase diagram of the solid solution $KNbO_3$ - $NaNbO_3$. The composition $K_{0.5}Na_{0.5}NbO_3$ is marked in the figure by a vertical green line. During the cooling from the liquidus state, the first solid phase that appears is cubic and paraelectric. Around 1100 ºC the composition is completely solid. The next phase transition occurs at 420 ºC and it is a phase transition (cubic to tetragonal) and a state transition (paraelectric

to ferroelectric). This is the Curie temperature of KNN. Close to 200 ºC, appears the tetragonal to orthorhombic phase transition and it remains like this until -150 ºC. At this temperature the system becomes rhombohedric. It was reported in the literature that the best piezoelectric properties of KNN are for 47.5 % of $KNbO_3$ [7]. Another important aspect to notice is that the transition temperatures almost do not change with the composition.

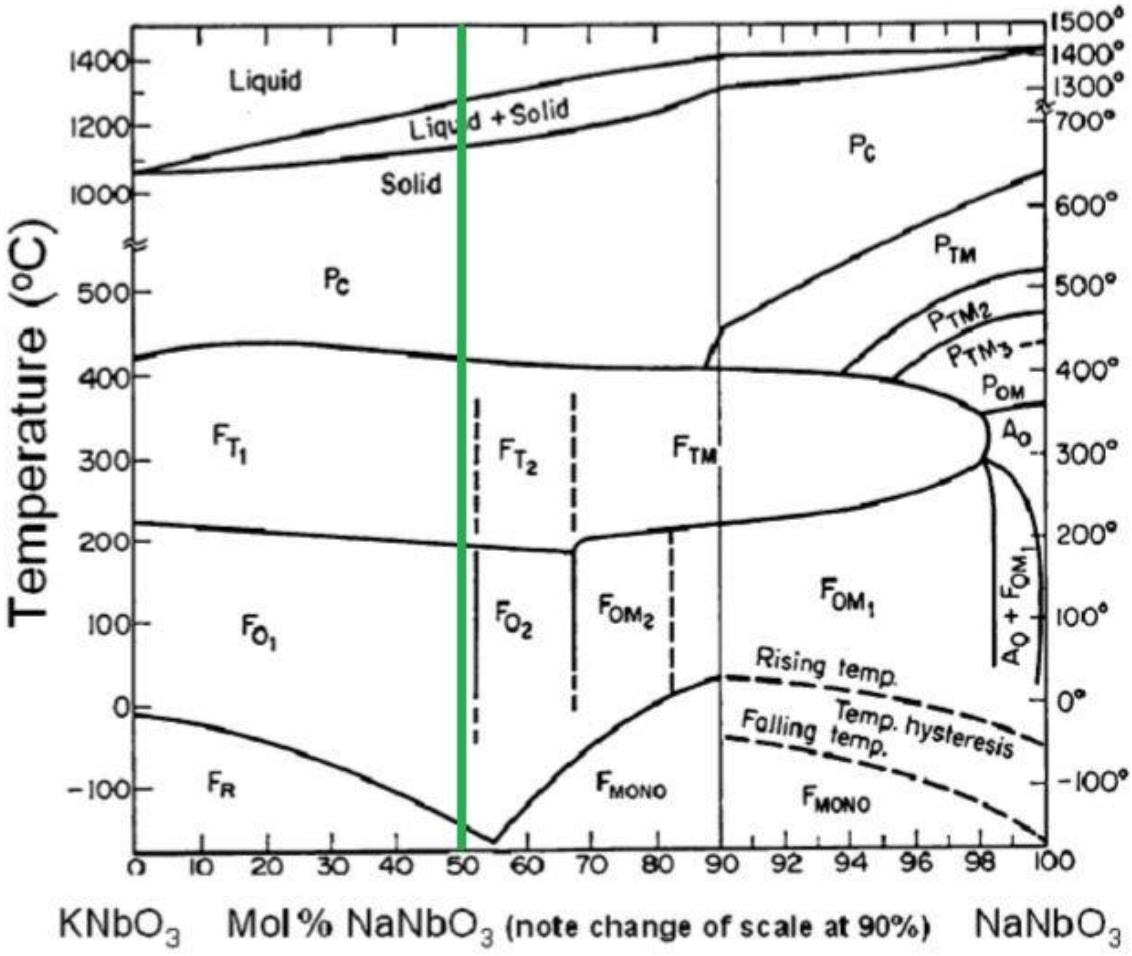

Figure 7 - Phase diagram of KNbO3-NaNbO3 system [13].

The maximum application temperature for piezoelectrics does not usually exceeds 1/2 of their T_C. Because of that, it becomes important to keep a high T_C [12].

Pure KNN when sintered by conventional mixed oxide processing, desirable for industrial applications, presents several limitations. The volatility of alkali elements, compositional heteroogeneity and poor densification are the most critical problems.

It was reported that KNN densification can be improved by manipulation of heating rate to be the most suitable 2 ºC/min [14]. However, the coupling coefficient drops down to approximately 50 % of the maximum value. Other techniques were tried out, like hot-pressing, and the coupling coefficient becomes higher than the value reported for conventional techniques, however the technique is expensive and not attractive for industrial applications. Spark plasma sintering was also tested, but an high temperature annealing is always needed to reduce the conductivity induced by the oxygen vacancies. In KNN ceramics produced by spark plasma sintering is important to notice the d_{33} = 148 pC/N and ε_r = 550.

In this work KNN ceramics were sintered with the assistance of dopants in order to contribute to solve some of these problems. The selected oxides were copper, lithium and manganese oxides.

Lithium oxide was reported as a sintering aid capable to improve density of KNN ceramics and to stabilize the dielectric properties. Mgbemere *et al.* reported that 0.2 and 0.4 % of lithium improves KNN densification to 91 % and 95 % of relative densification, respectively. It was also reported that, for this amount of lithium, sintering temperatures above 1100 ºC induces a decrease in densities due to the volatility of potassium and lithium related to their high vapor pressures. For concentrations higher than 0.4 % formation of secondary phases is promoted. Lithium ions occupy A site positions in perovskite structure due to its oxidation state and ionic radii (Li^+ = 90 pm, K^+ = 152 pm and Na^+ = 116 pm) [15].

Copper oxide was also reported as a sintering aid capable to improve KNN densification due to the formation of liquid phase at grain boundaries. Alkoy *et al.* demonstrated that the addition of 1.5 % of CuO promotes the formation of liquid phase in grain boundaries and increases the average grain size and density. The addiction of 1.5 mole % led to an increase of density from 89.3 % of relative densification for undoped KNN to an relative density of 97.8 %. Copper ions occupy B site of the perovskite structure, taking in consideration ionic radii (Nb^{+5} = 78 pm and Cu^{+2} = 87 pm). This substitution produces positively charged oxygen vacancies according to Equation 7 [1].

$$Nb_{Nb} + \frac{3}{2}O_O + CuO \rightarrow Cu''''_{Nb} + \frac{1}{2}Nb_2O_5 + \frac{3}{2}V_O^{\cdot\cdot} \quad \text{Equation 7}$$

The piezoelectric coefficient of KNN doped with 1.5% CuO is d_{33}=120 pC/N which is an improvement when compared with pure KNN (80 pC/N) [1-2].

The other sintering aid reported was manganese oxide (II) that affects positively KNN densification until certain amounts [16]. Manganese oxide is also quite well known as a dielectric losses suppresser. In systems, as $SrTiO_3$, BT, PZT and many other electroceramics, it was reported that the use of manganese increases densities, decreases dielectric losses and improves electromechanical properties [17-18]. Matsumoto *et al.* reported that the ideal amount of MnO doping for KNN is 0.5 %, more than that is followed by a density decrease. However, Kizaki *et al.* demonstrate in their investigations that manganese ions actually occupy B positions in perovskite structure, forming positively charged oxygen vacancies as can be described in Equation 8 [19]. It was reported also that manganese ions occupy B site based on the fact that lattice parameters of KNN single crystals increase with increasing dopant level, which can be explained by manganese ions being bigger than niobium ions (Nb^{+5} = 78 pm and Mn^{+2} = 97 pm).

$$Nb_{Nb} + \frac{3}{2}O_O + MnO \rightarrow Mn'''_{Nb} + \frac{1}{2}Nb_2O_5 + \frac{3}{2}V_O^{\cdot\cdot} \quad \text{Equation 8}$$

Table 1 presents that doped KNN can be the solution for properties improvement. It is important to notice that texturization has an important role also. Texturization is addressed is the following sub chapter. The composition LF4, present in Table 1, correspond to $(K_{0.44}Na_{0.52}Li_{0.04})(Nb_{0.86}Ta_{0.10}Sb_{0.04})O_3$.

Table 1 - Dielectric permittivity and piezoelectric coefficient (*d33*) for polycrystalline KNN, KNN single crystals, doped KNN and doped/textured KNN ceramics.

Composition	Dielectric permittivity (ε_r)	Piezoelectric coefficient (d_{33})	Ref.
KNN	290	80 pC/N	[13]
KNN single crystals		160 pC/N	[12]
KNN LF4		300 pC/N	[4]
KNN LF4T	1570	416 pC/N	[4]

Template grain growth (TGG)

The template grain growth process (TGG) uses single crystals to regulate the grain growth in a polycrystalline matrix to convert it into a single crystal-like growth in which a preferential crystallographic orientation dominates. TGG can be homoepitaxial or heteroepitaxial. TGG the single crystals or templates added to the matrix have the same composition and crystal structure of the matrix. On other hand, heteroepitaxial TGG method uses single crystals or templates with different composition, but with the same crystal structure of the matrix material In these methods, the large grains grow at the expense of the finer matrix ones, usually by a mechanism called Ostwald ripening [20].

The template grain growth starts once the density achieves 95 % of the theoretical densification because, as well known from the sintering theories, pores restrain boundary motion. The use of large template particles restrains densification as well. Therefore, one resorts to liquid phase during the sintering to accelerate the growth process.

In order to produce textured ceramics, a small proportion of templates must be homogeneously dispersed into a relatively fine grain size matrix. Initially the particles might be randomly oriented, but they should align during the green conformation. Indeed the TGG success depends on the initial alignment of the template particles, the epitaxial nucleation and the growth of these oriented particles during the high-temperature treatment [20].

The template particles must have a high-aspect ratio morphology, in order to be easily mechanically oriented during the green forming. Also, when texturing is performed for enhancement of physical properties, like dielectric permittivity or piezoelectricity, the template axis should match the desired crystallographic orientation. As mentioned before, most of the TGG processes include the presence of a liquid phase during the sintering process to improve the growth kinetics and, consequently, the template particles must be sufficiently stable in the presence of the liquid phase at high temperature.

In homoepitaxial TGG, where the template has the same composition of the matrix materials, the solubility of the material in the liquid phase is governed by Gibbs-Thompson equation (Equation 9).

$$S = S_0 exp\left(\frac{2\gamma M}{\rho r R T}\right)$$ Equation 9

where S is the solubility, S_0 is the solubility of the material for a particle with infinite radius, γ is the average surface energy, M is the molecular weight, ρ is the density of the material, r is the average grain size, R is the gas constant and T is the temperature. The large particles have lower solubility due to the solubility dependence on r ($r_{template} >> r_{matrix}$), which leads to Ostwald ripening process. In this case TGG process is dependent on the difference in particle size between templates and matrix.

The powder morphology used in matrix has equal importance to successfully achieve textured ceramics. The matrix must not chemically react with the template particles before the templates served their function, be in the final phase form, sinter to high density (> 95 % theoretical density) and have a smaller grain size than template particles after densification [20].

The matrix grain growth can reduce the driving force so that the template grain growth may stop. In order to avoid this effect, a large size difference between the matrix and the template particles must be considered. It was reported that the minimum size ratio that sustain template growth is ≈ 1.5, however, a larger size difference is preferred to avoid growth limitations [20].

As described before, the Saito *et al.* [4] work shows the best example of texturing in KNN ceramics by using (100)-preferentially oriented particles, achieving an increase from 300 pC/N to 416 pC/N (see Table 1).

In what concerns piezoelectrics, in some cases the residual presence of template particles inside the piezoelectric microstructure may negatively affect the piezoelectric and dielectric properties. Most of the works reported on KNN texturing used template particles from a different systems. In this work KNN single crystals were produced and texturing was accomplished by using KNN single crystals templates.

Experimental

In this chapter the experimental strategy used along the work is presented in detail (Figure 8). The preparation procedure of the materials under study is described, who includes the preparation of polycrystalline KNN ceramics, the growth of KNN single crystals and preparation of textured KNN ceramics. This description is followed by the presentation of the major experimental techniques used to characterize the structure, microstructure, dielectric and piezoelectric properties.

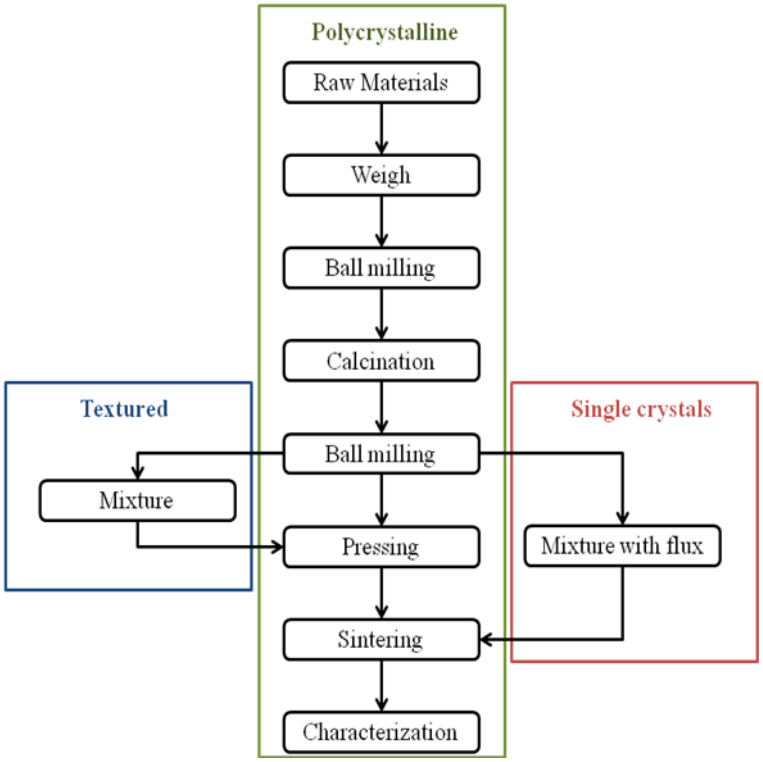

Figure 8 - Flowchart of the work carried out in this work.

Polycrystalline and textured KNN bulk ceramics were prepared by conventional ceramic processing that includes the synthesis of the compositions by solid state reaction method, milling, pressing and sintering of ceramic disks. KNN single crystals were grown by flux method, according to a previously reported methodology [12], to be used as templates for texturing KNN ceramics. The compositions under study are indicated in Table 2. The raw materials used in this work are shown in Table 3.

Table 2 - KNN compositions under study.

Compositions
$((K_{0.5}Na_{0.5})_{0.98}Li_{0.02})(Nb_{0.985}Cu_{0.015})O_3$
$((K_{0.5}Na_{0.5})_{0.96}Li_{0.04})(Nb_{0.985}Cu_{0.015})O_3$
$(K_{0.5}Na_{0.5})(Nb_{0.98}Cu_{0.015}Mn_{0.005})O_3$

Table 3 - Raw materials used for preparation of KNN bulk ceramics and single crystals.

Chemical name	Chemical formula	Purity	Source
Potassium carbonate	K_2CO_3	≥99%	Merck
Sodium carbonate	Na_2CO_3	≥99.5%	Chempur
Niobium oxide	Nb_2O_5	99.9%	Chempur
Copper oxide	CuO	99.9%	Aldrich
Lithium carbonate	Li_2CO_3	99%	Merck
Manganese oxide	MnO	99%	Aldrich

Polycrystalline KNN ceramics

Polycrystalline KNN bulk ceramics with compositions $(K_{0.5}Na_{0.5})_{1-x}Li_xNb_{1-y}Cu_yO_3$ (x=0.02 and 0.04; y=0.015) and $(K_{0.5}Na_{0.5})Nb_{1-x-y}Mn_xCu_yO_3$ (x=0.005; y=0.015) were prepared by conventional mixed oxide route. Figure 8 illustrates the used synthesis route for polycrystalline KNN ceramics.

The precursor powders were weighed in order to satisfy the above-mentioned compositions, and ball milled / mixed in Teflon® pots with zirconia balls in ethanol for 5 hours. The powders were then dried at 150 ºC for 12 h. Dried powders were pressed in form of pellets of 10 mm diameter first by uniaxial pressing at 170 MPa and after by cold isostatic pressing at 200 MPa.

KNN single crystals

KNN single crystals with the composition $(K_{0.5}Na_{0.5})NbO_3$ were prepared by flux method. In Figure 8 can be seen the route followed in schematic process.

The selected flux for the growth of KNN single crystals was a mixture of K_2CO_3 and B_2O_3 (weight ratio 9:1). The pre-calcined KNN powders (as described above) and the flux were mixed (weight ratio 4:1) by a ball milling for 5 h with zirconia balls and ethanol as the milling media. Then, 60 g of this mixture was loaded into a Pt crucible and sealed with a Pt lid. Pt crucible was filled in with ≈75% of the total volume, in order to avoid over-pressure inside the crucible. Then the Pt crucible was placed in a refractory alumina basis and covered with a larger alumina crucible, as illustrated in Figure 9. The thermal cycle used is depicted in Figure 10. The cycle starts with a relative high heating ratio (150 ºC/min until 1000 ºC and 50 ºC/min up to 1250 ºC) and then stays at 1250 ºC for 10 h. After, the cooling is very slow from 1250 ºC to 600 ºC, and increases to 150 ºC/min again. Note that the entire cycle takes close to 83 h.

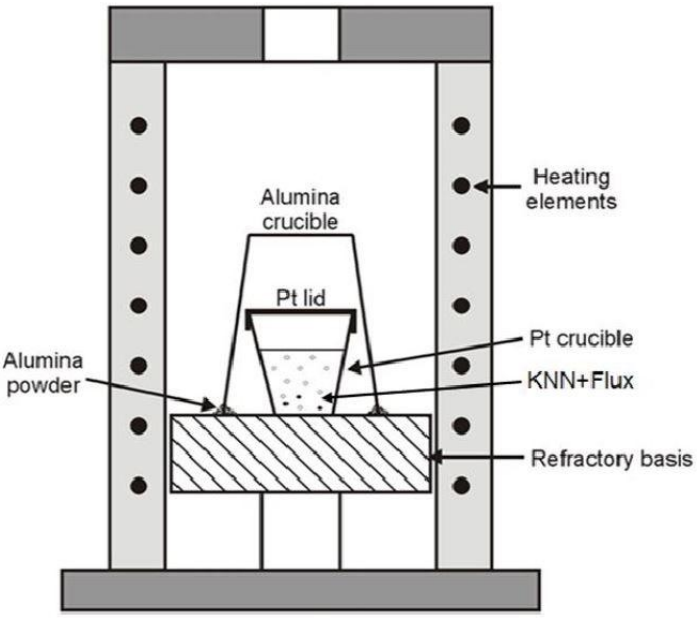

Figure 9 - Schematic representation of the furnace and crucible positions used for the growth KNN single crystals.

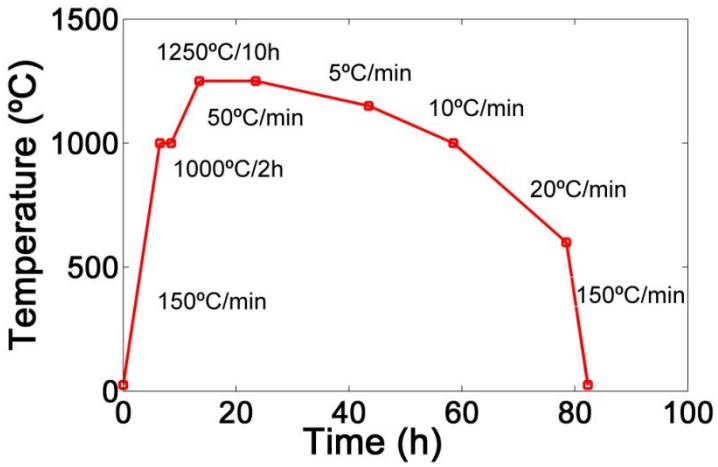

Figure 10 - Thermal profile used for the growth of KNN single crystals.

After the growth, the crystals were left in water for several days in order to dissolve the remaining flux. Then crystals were cleaned again in fresh water in a ultra-sonic bath for several times. The crystals were then crushed and sieved (325 mesh) to be used in the KNN textured ceramics [12].

Textured KNN ceramics

KNN textured ceramics with compositions $(K_{0.5}Na_{0.5})_{1-x}Li_xNb_{1-y}Cu_yO_3$ (x=0.02 and 0.04; y=0.015) and $(K_{0.5}Na_{0.5})Nb_{1-x-y}Mn_xCu_yO_3$ (x=0.005; y=0.015) were prepared by conventional mixed oxide route. Figure 8 presents the processing route of textured KNN ceramics.

Polycrystalline KNN powders previously prepared were mixed with 10 wt% of crushed single crystals and stirred in ethanol for 2 h in order to achieve homogeneity. Then the mixture was dried in air at 120 ˚C for 12 h. Dried powders were pressed in form of pellets of 10 mm diameter first by uniaxial pressing at 170 MPa and after by cold isostatic pressing at 200 MPa. KNN textured ceramics were sintered under the same conditions as the polycrystalline KNN bulk ceramics for further comparison, as described below.

Sintering conditions

In what concerns the sintering conditions the work was divided in two main parts. In Part I untextured and textured KNN of the previously indicated compositions were sintered. The chosen sintering conditions were 2 ºC/min for heating and cooling rate, 2 h of dwell time at the following sintering temperatures: 1050 ºC, 1065 ºC and 1080 ºC. The sintering was conducted in air. In part II the main objective was to improve the degree of texturization and to evaluate the role of some processing parameters in the texturization process. For this purpose only one composition ($(K_{0.5}Na_{0.5})(Nb_{0.98}Cu_{0.015}Mn_{0.005})O_3$) and one sintering temperature (1065 ºC) were chosen. The amount of added single crystals was 2.5 wt%, 5.0 wt% and 10 wt%, the heating / cooling rate was 2 ºC/min, 10 ºC/min and 20 ºC/min and the dwell time varied from 4 to 24 h.

Experimental techniques

X-Ray diffraction (XRD)

X-ray diffractograms were obtained at room temperature using X-ray powder diffraction (XRD, Rigaku, D/Max-B, Cu-Kα radiation; λ=0.15064 nm). The XRD analysis was carried out at 50 kV and 30 mA and θ-2θ scans at 1˚/min between 20-60˚.

The degree of crystal orientation was evaluated in terms of the Lotgering Factor (*f*) according to Equation 10:

$$f(h00) = \frac{P(h00) - P_0(h00)}{1 - P_0(h00)} \qquad \text{Equation 10}$$

where, $P = \sum I_{h00} / \sum I_{hkl}$ and $P_0 = \sum I^0_{h00} / \sum I^0_{hkl}$, with I_{hkl} and I^0_{hkl} being the intensities of (hkl) peaks for the textured and randomly oriented samples, respectively.

Scanning electron microscopy (SEM)

The microstructure was analysed using a SEM, S4100, Hitachi, Tokyo, Japan, coupled with EDS (QUANTAX 400, Bruker, Berlin, Germany).

The polished and etched sections of the sintered samples were prepared according to the following steps. Small pieces of samples were firstly inserted in resin and, after a coarse polishing with silicon carbide paper, the surfaces were polished using a sequence of fine diamond pastes (15 μm, 6 μm, 3 μm, 1 μm and 0.25 μm) until a mirror like surface was achieved. The polished samples removed from the resin were thermally etched at temperatures 50 ºC below the corresponding sintering temperature for 45 min. Etched samples were glued to SEM holders using carbon tape and carbon was sputtered on the samples surface to perform the SEM analysis, using a Emitech K950 carbon depositor.

Image analysis of the acquired SEM micrographs was performed using ImageJ [21] and grain size and grain size distribution was calculated. For that 3 images were used and a minimum of 600 grains were measured. For the use of ImageJ the grain areas were manually drawn and then the SEM micrographs were modified in the following way: contrast enhancement, median filtering and thresholding in order to achieve binary suitable images; the grain size and grain size distribution were automatically calculated.

Dielectric measurements

The complex permittivity at RF frequency was measured as a function of the temperature and frequency in a capacitive cell as illustrated in Figure 11.

For the case of sinusoidal applied voltage *V*, the current discharge flow I of the capacitive cell can be written as:

$$I = \frac{i\omega\varepsilon^* V\varepsilon_0 S}{ds} = \frac{i\omega(\varepsilon' - i\varepsilon'')V\varepsilon_0 S}{ds} = I_C + I_R \qquad \text{Equation 11}$$

where i stands for the imaginary operator, $\omega = 2\pi f$ for the angular frequency, ε_0 for the relative permittivity of the vacuum with the value 8.85×10^{-12} F/m, *S* for the area of the electrodes for a planar capacitor, *ds* for the distance between electrodes or sample

thickness, ε^* for the complex permittivity, ε' for the real part of the permittivity, and ε'' is the imaginary part of the permittivity, related to the dielectric loss. The dielectric loss existing in a dielectric material can then be represented by the analogue circuit of a resistance in parallel with a capacitor, and being *IC* and *IR* of the vector components the current of the *IC* and *IR*, as illustrated in Figure 11(b, c). The *IC* current represents a capacitive current proportional to the charge stored in the capacitor. It is frequency dependent. The current *IR* is an ac conduction current in phase with the voltage *V*, which represents the energy loss or power dissipated in the dielectric. The dissipation factor is defined as tanδ = ε"/ε' [22].

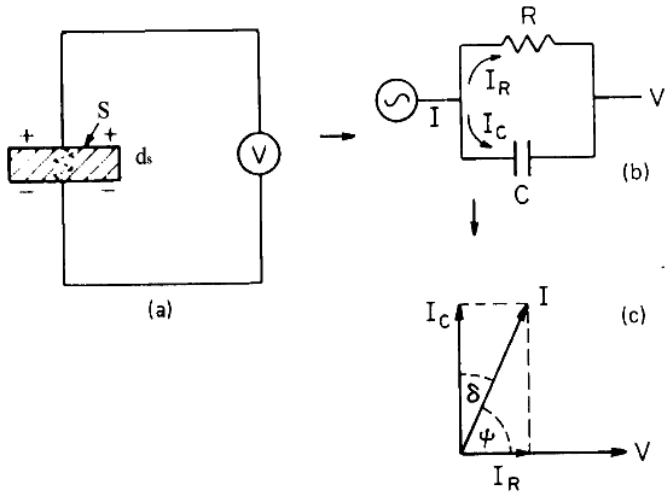

Figure 11 - Equivalent circuit diagrams of capacitive cell (a) of charging and loss current (b) and of loss tangent for a typical dielectric (c) [22].

In this work, the electrical measurements at RF frequency were conducted via a metal-insulator-metal (MIM) configuration using Au as the top electrode. The ceramics were polished until 0.8 mm thickness, and top and bottom Au electrodes of 6 mm diameter were sputtered. The electrical properties were measured from 500 ºC to room temperature using a Hewlett-Packard precision LCR Meter (Model HP 4284A) connected to a PC via a GPIB card and working in the frequency range from 100 Hz to 1 MHz. The heating / cooling was performed in a vertical furnace and the temperature was controlled by an Eurotherm 2404 controller and a thermocouple placed very close to the sample in order to increase the temperature precision. For each composition and set of conditions three measurements were performed. The analysed electrical properties include the relative permittivity and loss tangent.

Piezoelectric coefficient

Generally there are four methods for measuring piezoelectric coefficients: direct measurements of stress-induced charge (Berlincourt method), laser interferometers, laser scanning vibrometers, and piezoelectric force microscopes. For bulk ceramic materials, the most commonly used method to characterize the piezoelectric coefficients are based on a method using a dynamically varying load, the Berlincourt meter [23]. This was the method used in this work. In addition, this is the method universally accepted by the piezoelectric industry for bulk piezoelectrics.

Piezoelectric coefficient (d_{33}) is an important parameter from the application point of view of KNN materials. In this work the direct piezoelectric coefficient was measured by Berlincourt meter, Sinocera, YE 2730A and a fixed force of 250 x 10^{-3} N was applied. A schematic representation of the equipment is shown in Figure 12. For the piezoelectric activation the ceramics must be polarized. In this work the samples were polled above 3.5 kV/mm for 30 min using a oil bath at room temperature. The poled samples to be tested were placed between the two probes and the force applied.

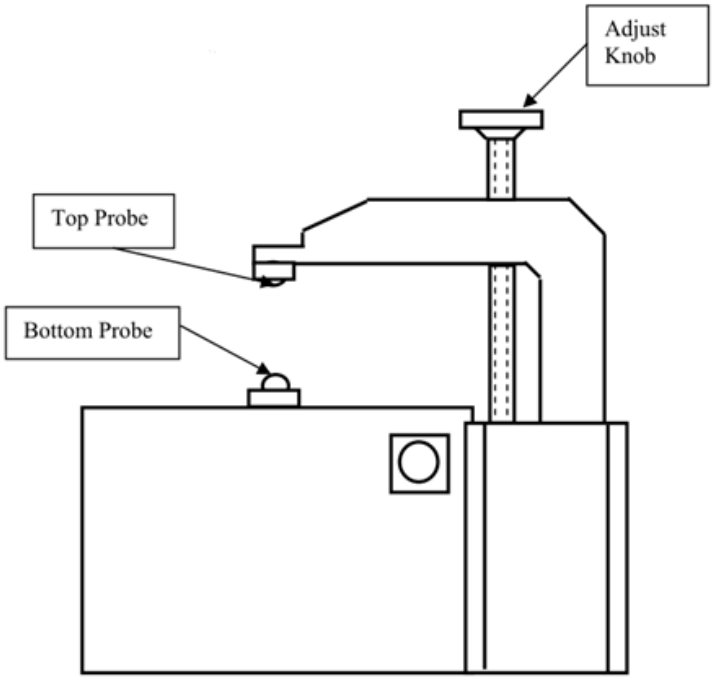

Figure 12 - Schematic representation of the Berlincourt.

Results and Discussion

Part I

Abstract

In order to fulfill the objectives of the work, in this part the effect of dopants and sintering temperature on the texturization of KNN ceramics was studied. For this study the selected compositions were (Table 2) i) KNN + 1.5 mol% CuO + 2 mol% Li_2O, ii) KNN + 1.5 mol% CuO + 4 mol% Li_2O and iii) KNN + 1.5 mol% CuO + 0.5 mol% MnO. 10 wt% of KNN single crystals was used for each composition. The sintering temperatures were: 1050 ºC, 1065 ˚C and 1080 ºC and the sintering was conducted in air with an heating rate of 2 ºC/min with 2 h of dwelling time.

The initial powders morphology, structure and phase assemblage was characterized. The density by Archimedes method, phase assemblage and degree of textured of the sintered KNN ceramics was evaluated and quantified. The dielectric and piezoelectric properties of KNN ceramics were measured. The relations between composition, processing variables and dielectric and electromechanical response were established.

KNN single crystals and powder characterization

Figure 13 shows the X-ray diffraction pattern of KNN single crystals used for texturing and the indexed diffraction planes of the KNN phase, according to PDF card 00-061-0315. Within the detection limits of the XRD equipment, KNN single crystals are monophasic. In the single crystal patterns the intensity of the peaks corresponding to (100) and (200) Miller index crystallographic planes is relatively higher when compared with the relative intensity of the peaks from the PDF file. This is due to the preferential orientation of the single crystals along these planes.

Figure 14 presents as grown KNN single crystals inside the platinum crucible and after being removed from the crucible and before the washing step. The size of single crystals

reached several millimeters. Figure 15 shows a SEM micrograph of crushed KNN single crystals after washing and sieving.

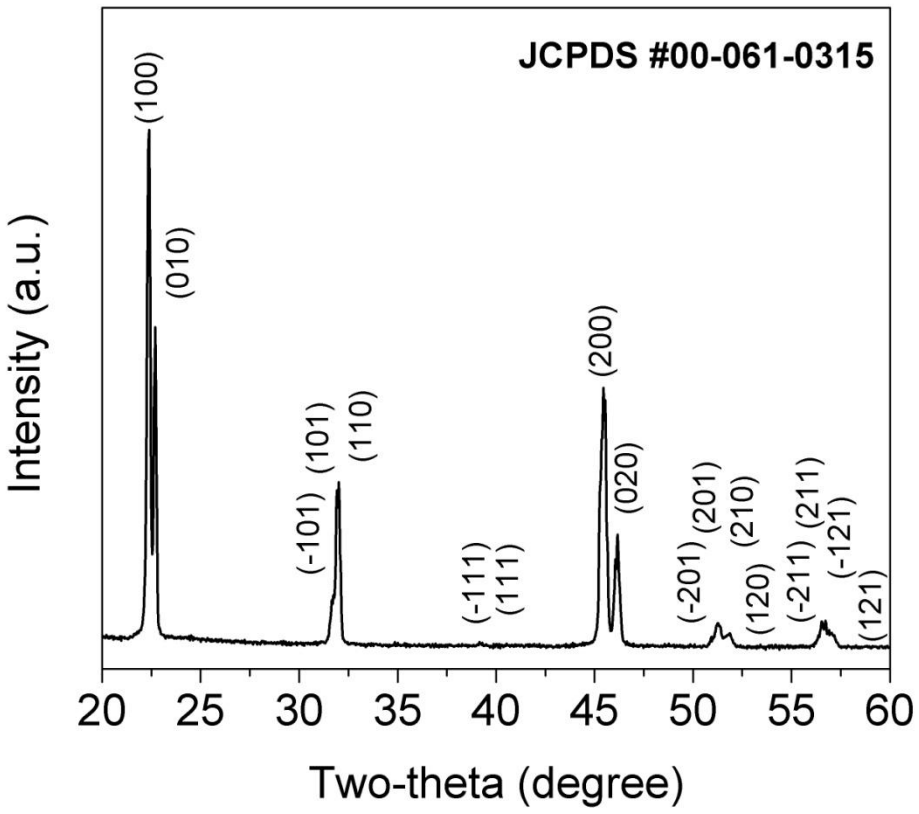

Figure 13 - X-ray diffraction of KNN single crystals used for texturing and crystallographic planes from the PDF card 00-061-0315.

Figure 14 - Photograph of KNN single crystals inside de platinum crucible (left) and KNN single crystals after removing from of the platinum crucible (right).

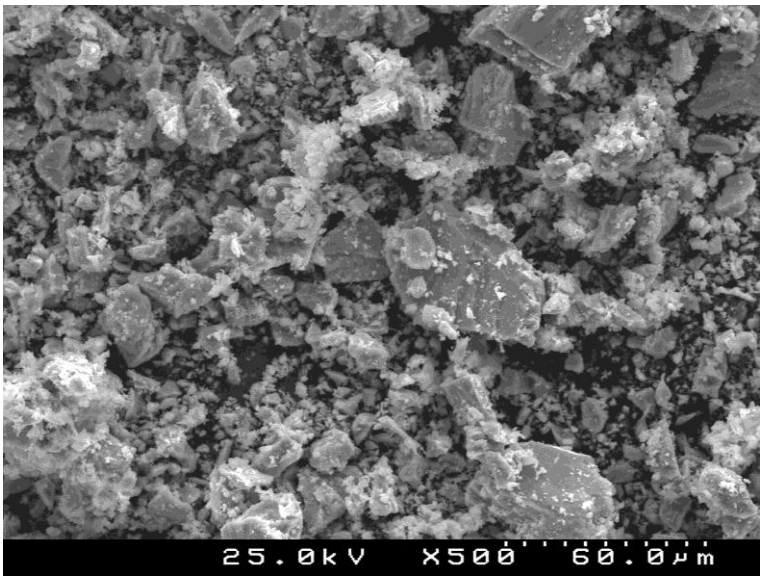

Figure 15 - SEM micrograph of crushed KNN single crystals after sieving.

The phase assemblage of calcined KNN powders was also analyzed by XRD (Figure 16). KNN crystallizes with a monoclinic structure (JCPDS 00-061-0315).

Undoped KNN powders are single phase and for the doped compositions secondary phases can be found. The secondary phase in KNN ceramics is usually attributed to pyrochlore phase ($KNaNb_2O_7$). Also was observed that the compositions with lithium present higher amounts of secondary phase and within the compositions doped with lithium, the amount of secondary phase increases with the increase of lithium added.

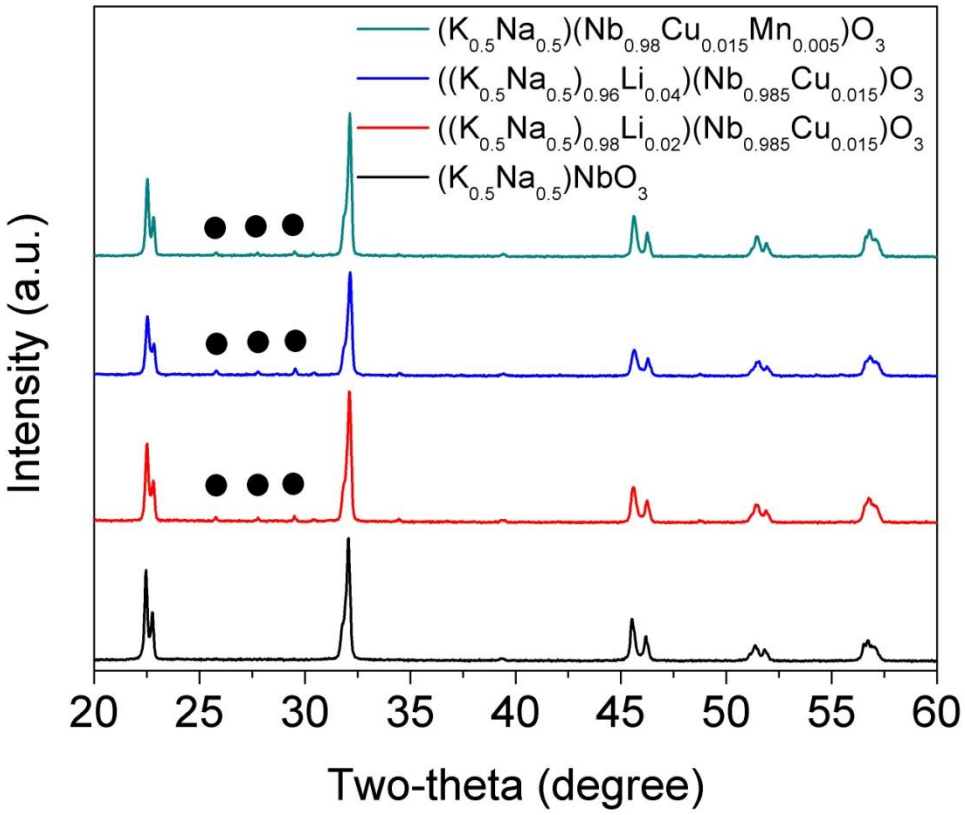

Figure 16 - X-ray diffraction patterns of doped and undoped KNN powders after calcination.

Figure 17 shows SEM micrographs of powders used in this work after milling. The KNN and KNN copper and lithium doped $(((K_{0.5}Na_{0.5})_{0.98}Li_{0.02})(Nb_{0.985}Cu_{0.015})O_3$ and $((K_{0.5}Na_{0.5})_{0.96}Li_{0.04})(Nb_{0.985}Cu_{0.015})O_3$) and KNN copper and manganese doped $((K_{0.5}Na_{0.5})(Nb_{0.98}Cu_{0.015}Mn_{0.005})O_3$) powders exhibit cube-like particles.

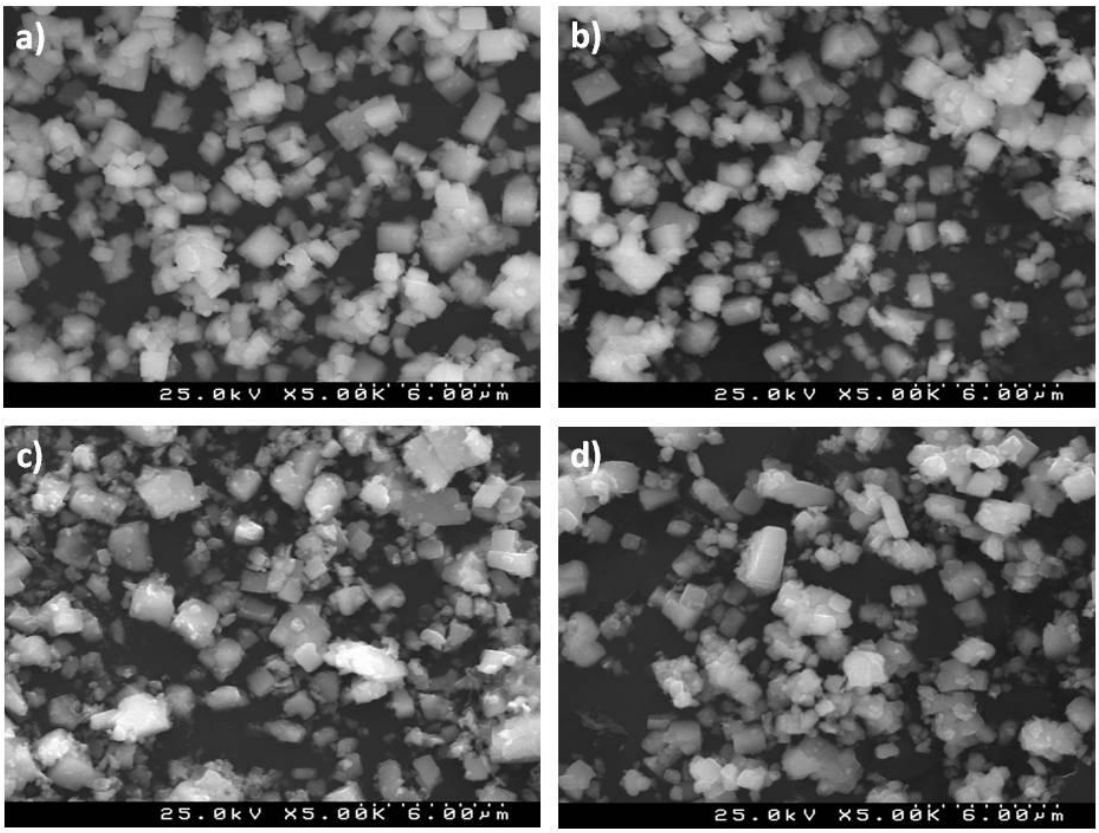

Figure 17 - SEM micrographs of KNN powders; a) KNN, b) KNN + 1.5 % CuO + 2 % Li_2O, c) KNN + 1.5 % CuO + 4 % Li_2O, d) KNN + 1.5 % CuO + 0.5 % MnO.

Figure 18 shows the particle size distribution of KNN powders (doped and undoped) in water. The particle size of the milled KNN calcined powders is below 7 μm. All the particle size distributions are characterized by a bimodal distribution with the highest volume % of particles showing a peak centred around 2 μm, but with a similar volume fraction of small particles below 1 μm, with the lower peak around 0.2 μm. There are no significant variations in the particle distributions between the different powders. This allow us to mention that future differences in the sintering behavior cannot be related with differences in particle size distribution of the powders.

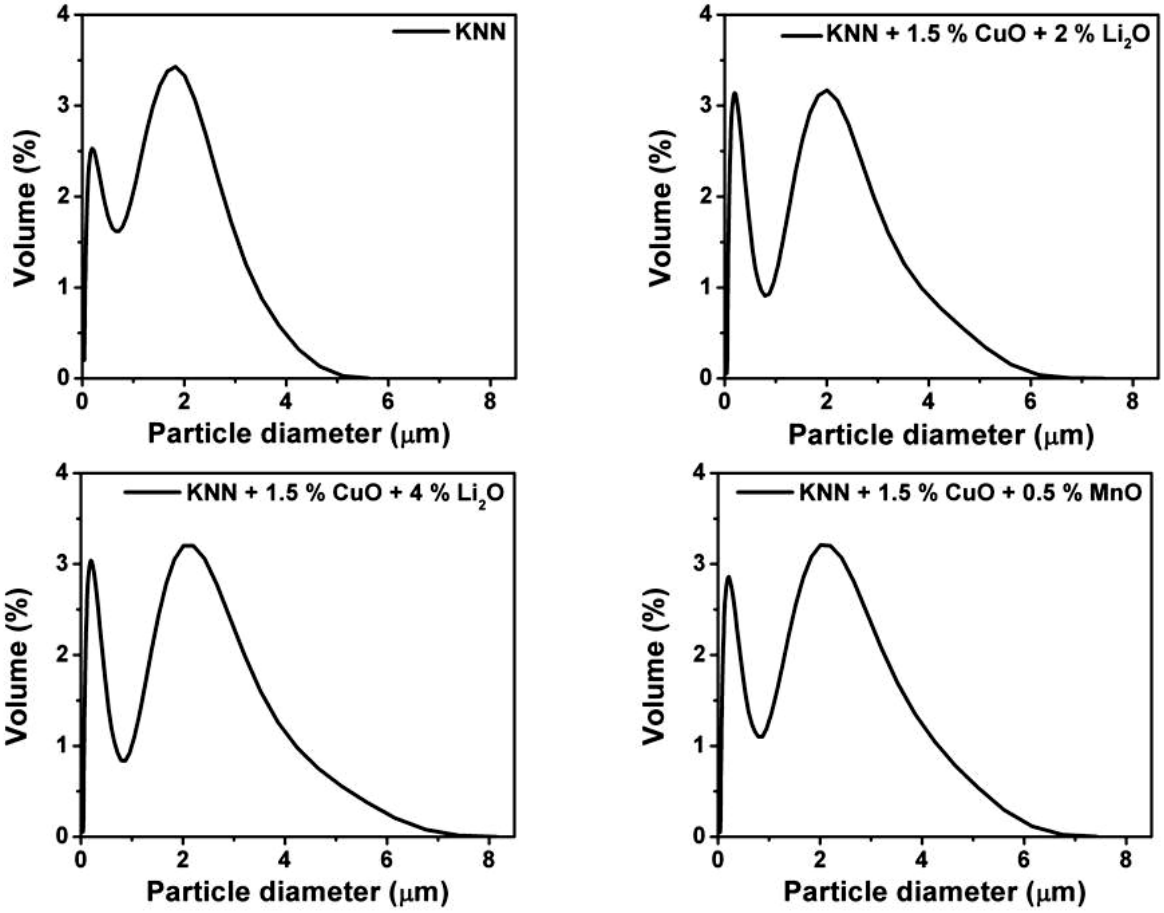

Figure 18 - Particle size distribution of KNN powders (doped and undoped).

The densification, in terms of the percentage of A_l/L_0 obtained from the dilatometric analysis is represented as a function of temperature, *T*, in Figure 19.

Up to 1050 ºC, undoped KNN has a low shrinkage (≈ 5 %) when compared with any doped KNN compositions (15-17 %). Note that the presence of lithium lowers the temperature at which KNN starts to shrink from ≈800 ºC to ≈700 ºC. This is an indication of the sintering aid role of lithium, related with the increase of liquid phase. In the case of composition doped with copper and manganese, it can be observed that the shrinkage temperature remains close to 800 ºC, the shrinkage occurring after that temperature.

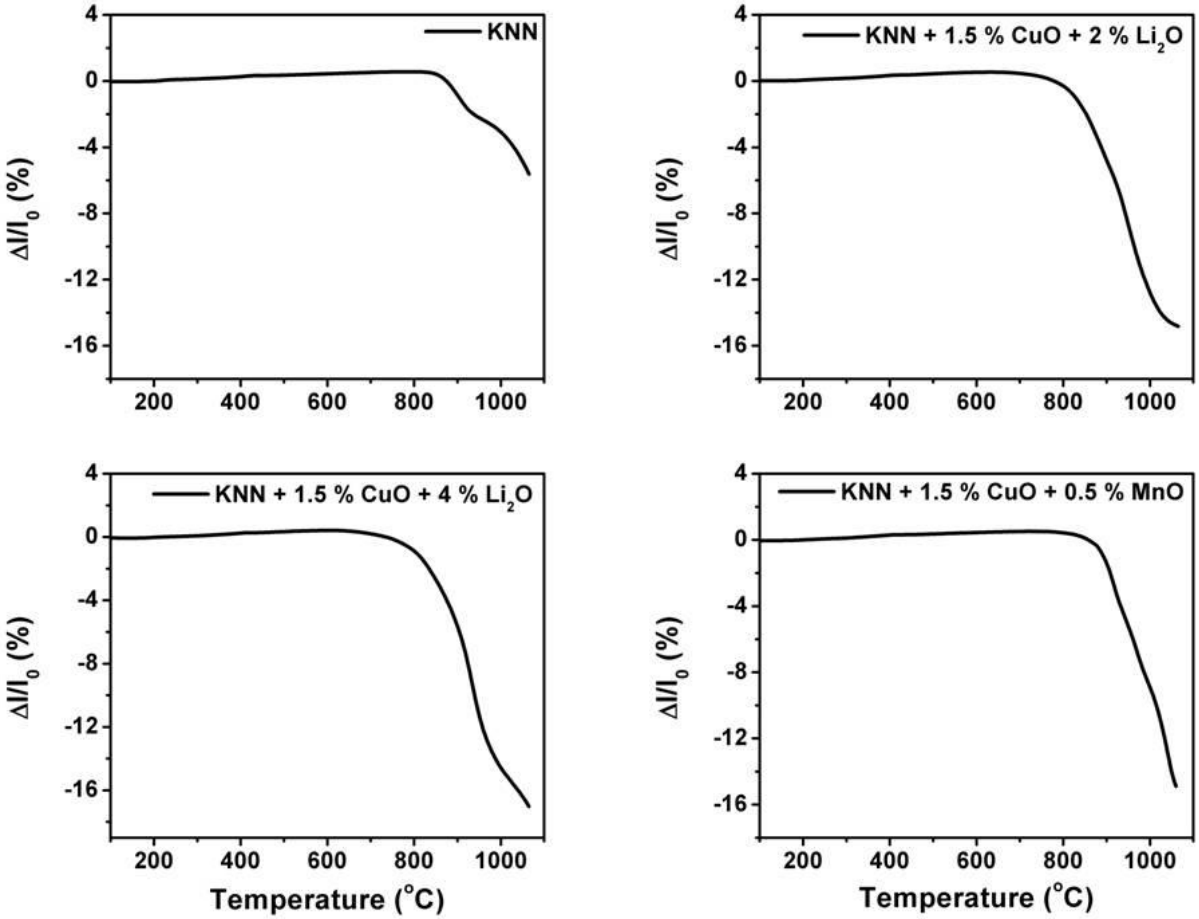

Figure 19 - Dilatometry curves for pure and doped KNN.

Untextured doped KNN ceramics

X-ray diffractograms of bulk KNN sintered at distinct temperatures are presented in Figure 20, 21 and 22, KNN+1.5% CuO+2% Li_2O, KNN+1.5% CuO+4% Li_2O and KNN+1.5% CuO+0.5% MnO, respectively. The compositions with copper and lithium oxides exhibit secondary phase in the samples sintered at 1050 ºC. The composition with copper and manganese oxide shows single phase for all temperatures studied.

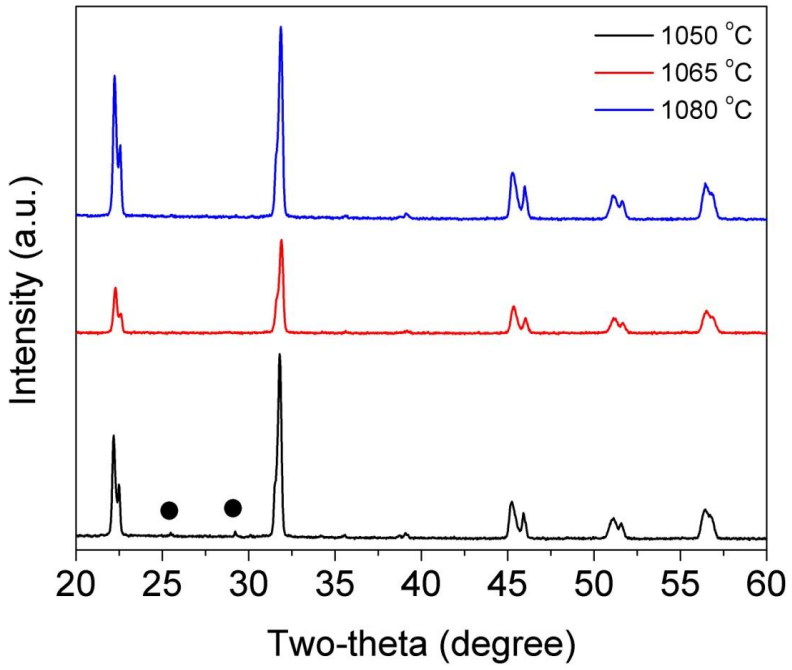

Figure 20 - X-ray diffraction patterns of the samples of KNN+1.5% CuO+2% Li2O sintered at different temperatures.

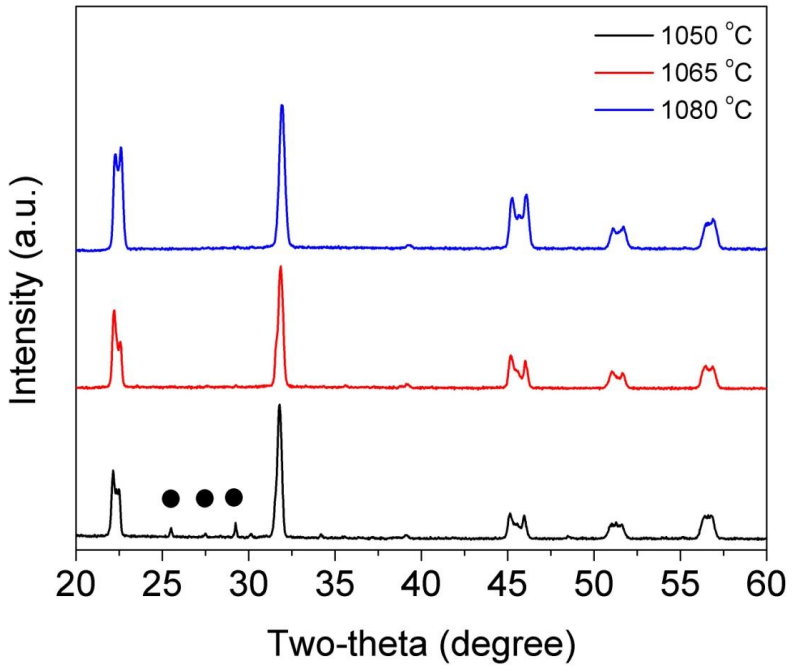

Figure 21 - X-ray diffraction patterns of the samples of KNN+1.5% CuO+4% Li_2O sintered at different temperatures.

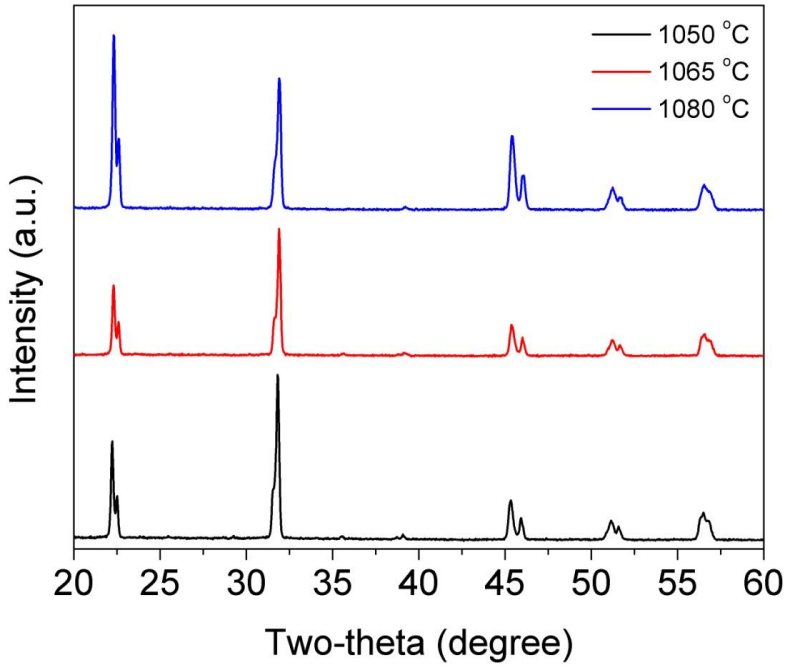

Figure 22 - X-ray diffraction patterns of the samples of KNN+1.5% CuO+0.5% MnO sintered at different temperatures.

The relative density of the different compositions sintered at different temperatures is depicted in Figure 23. All the samples exhibit densities above 95 %. The compositions doped with copper and lithium show the highest densities. On the other hand KNN doped with copper and manganese (KNN+1.5% CuO+0.5% MnO) exhibits the lowest density for the highest sintering temperature. The highest achieved density is 98.7% for copper and 4% lithium doped KNN, sintered at 1080 ºC. These results are in agreement with the dilatometers (Figure 19).

In comparison with undoped KNN, even for the lowest density that is higher than 95%, these doped samples are dense; the undoped KNN densification problems can be solved with the help of these dopants.

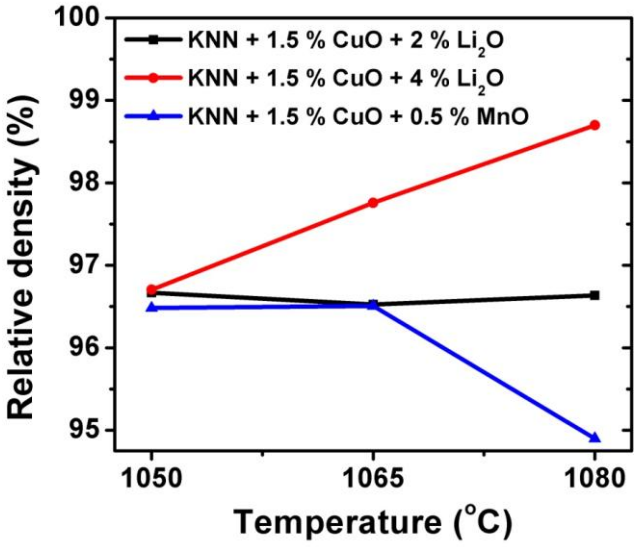

Figure 23 - Relative densities of doped KNN ceramics sintered at different temperatures.

The SEM micrographs of doped KNN compositions sintered at different temperatures are displayed in Figure 24. For comparison all the micrographs have the same magnification. In agreement with the relative densities (Figure 23) these doped ceramics are characterized by dense microstructures. Li doped KNN ceramics are denser than the Mn doped ones. As expected, as the sintering temperature increases the density increases and the grain size as well; the Mn based composition presents the smaller grain size. Figure 25 shows the grain size distribution for the different KNN compositions sintered at different temperatures that support the SEM observations. For the compositions doped with copper and lithium, the increase of lithium content increases the average grain size for the same temperature what may be related to the increase of the amount of liquid phase generated during sintering. The composition doped with copper and manganese exhibits the lowest average grain size. In all the compositions an increase of grain size with the increase of sintering temperature can be observed.

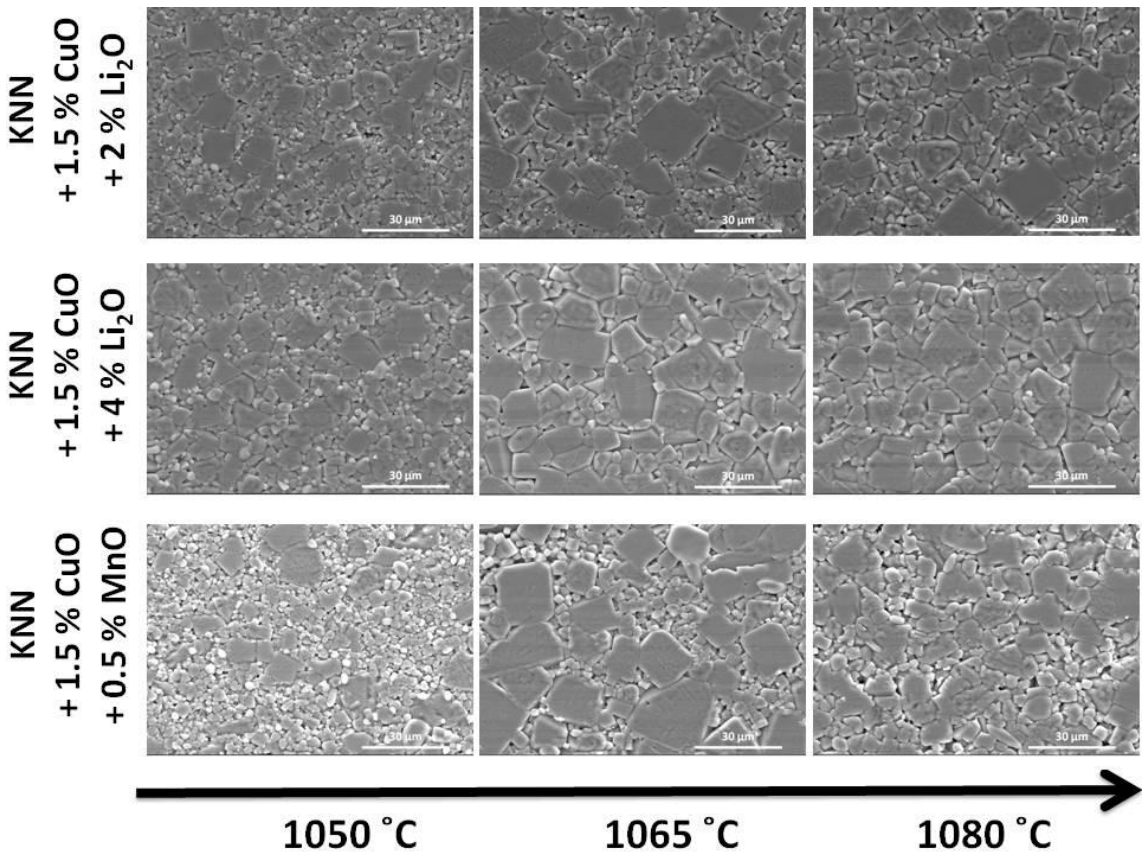

Figure 24 - SEM micrographs of doped KNN sintered at different temperatures.

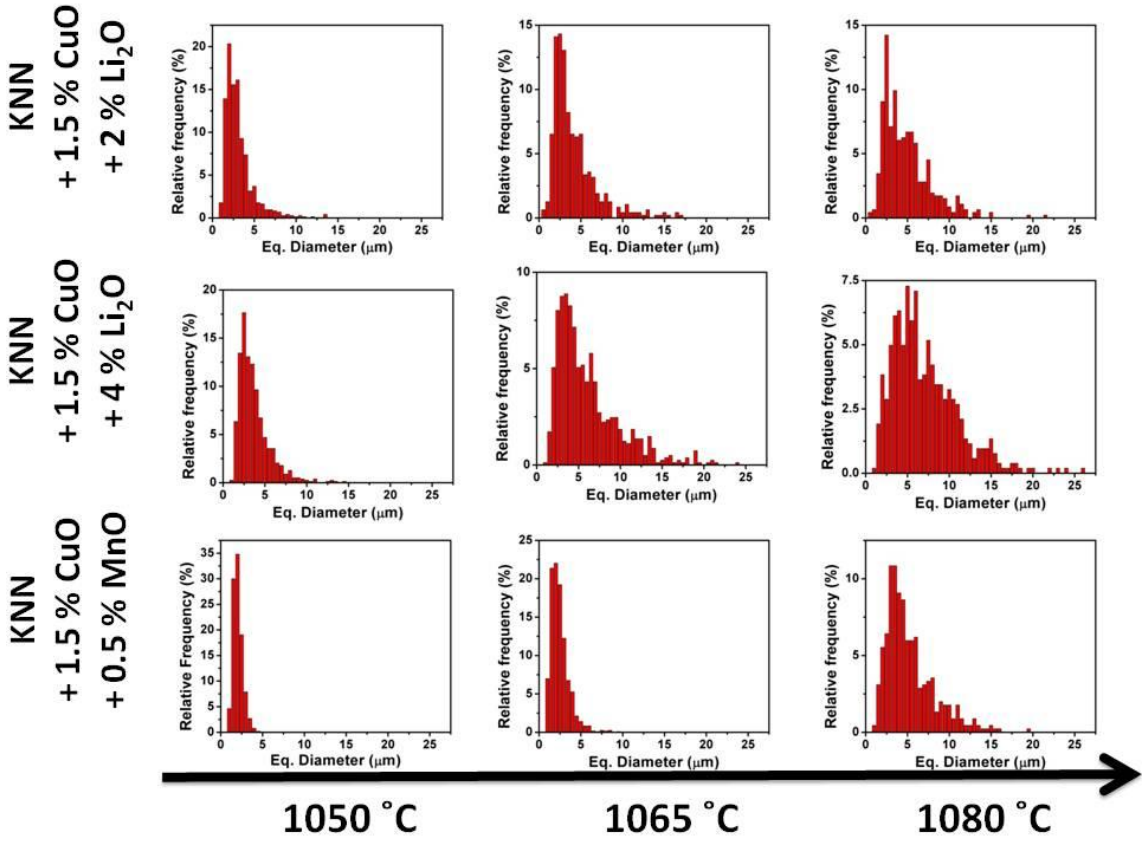

Figure 25 - Grain size distribution of doped KNN for different temperatures.

Textured doped KNN ceramics

XRD patterns of textured ceramics of the different compositions are presented in Figure 26, 27 and 28, for KNN+1.5% CuO+2% Li_2O, KNN+1.5% CuO+4% Li_2O and KNN+1.5% CuO+0.5% MnO, respectively. The compositions with copper and lithium oxide exhibit extra phases in the samples sintered at 1050 ºC. For higher temperatures the secondary phase is not visible. The composition with copper and manganese oxide shows single phase for all the studied temperatures. It can be seen that the relative intensity of (h00) peaks is higher comparing with the untextured samples. This profile is closer to the pattern founded in KNN single crystals (Figure 13).

Lotgering factor was calculated for each sample and the degree of texturing is presented in Figure 29. The Lotgering factors varied between 4 % and 19 %. The composition doped with copper and manganese show a higher preferential orientation along (h00)

direction and the highest Lotgering factor was calculated for the sample sintered at 1065 ºC (≈19 %). This value is 2 times higher than any of the copper and lithium doped samples.

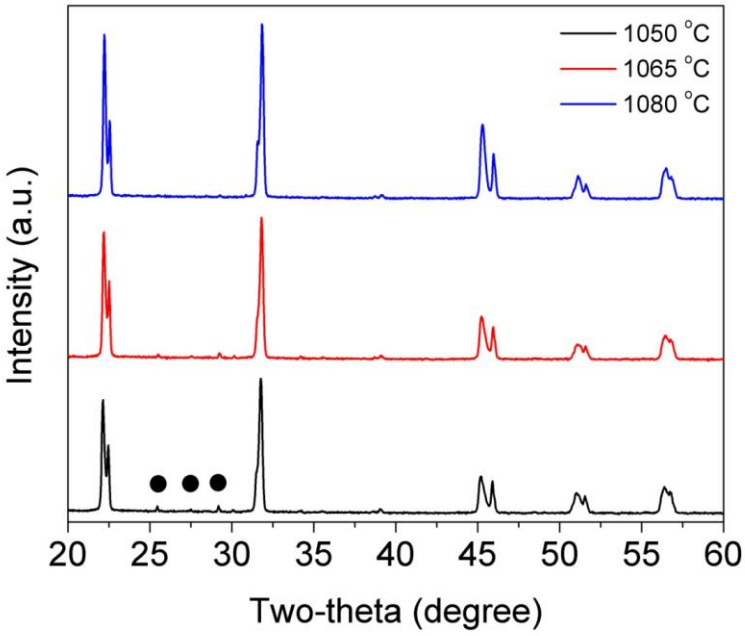

Figure 26 - X-ray diffraction patterns of the samples of textured KNN+1.5% CuO+2% Li_2O sintered at different temperatures.

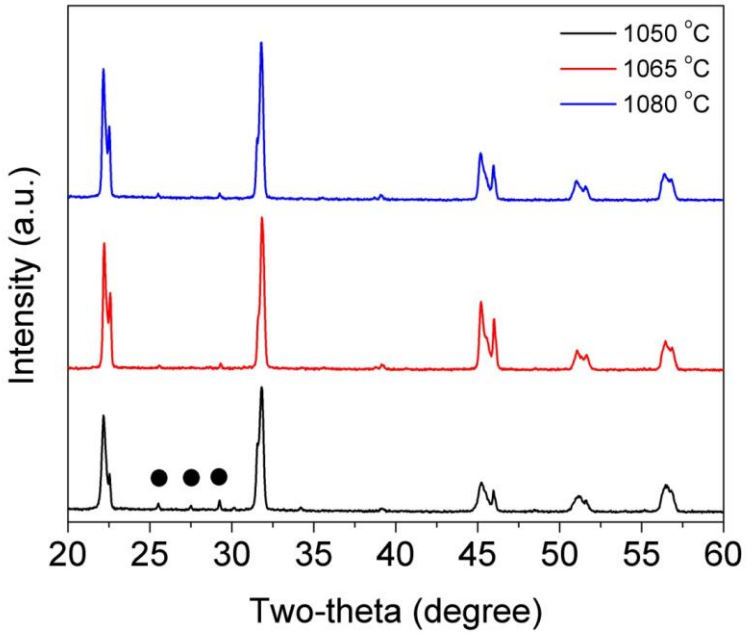

Figure 27 - X-ray diffraction patterns of the samples of textured KNN+1.5% CuO+4% Li_2O sintered at different temperatures.

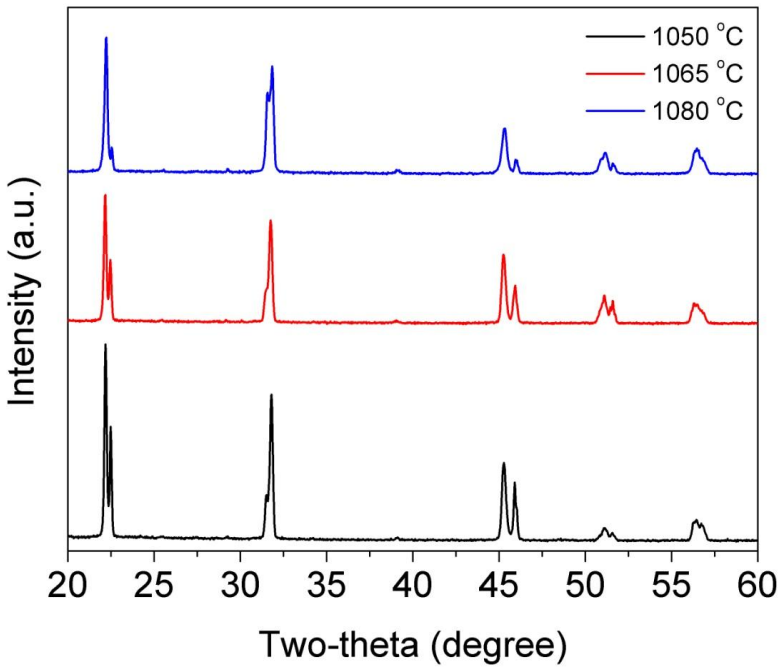

Figure 28 - X-ray diffraction patterns of the samples of textured KNN+1.5% CuO+0.5% MnO sintered at different temperatures.

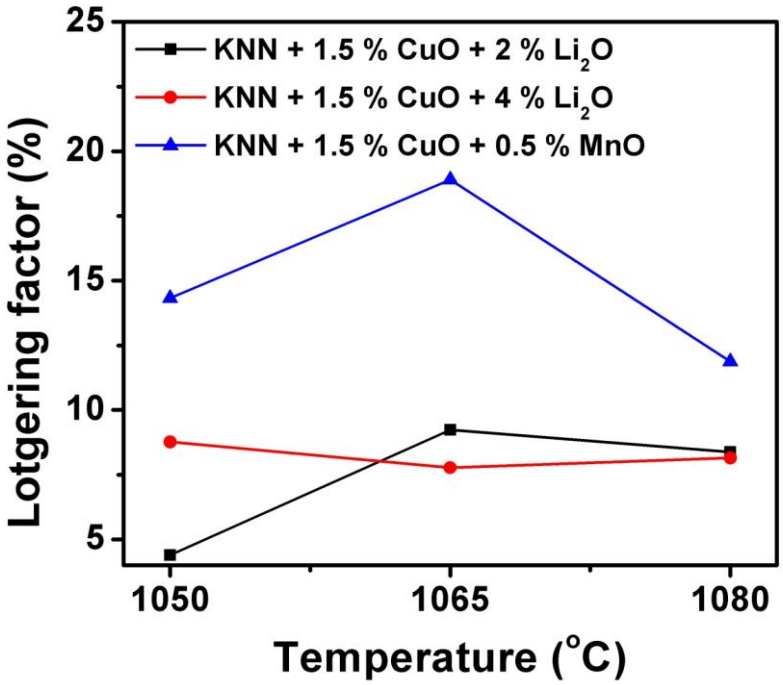

Figure 29 - Lotgering factor (%) for textured doped KNN sintered at different temperatures.

Figure 30 shows the relative density of the different textured compositions sintered at different temperatures. As observed for the untextured compositions, textured ceramics doped with copper and lithium show the highest densities above 1065 ºC. It can be seen that textured KNN doped with copper and manganese possess the lowest density for 1065 ºC. It is important to notice that for temperatures above 1065 ºC the lowest density is higher than 96%, this means that all of these samples are quite dense. The highest density is 99.6% for copper and 2% lithium doped KNN, sintered at 1080 ºC. Note that for untextured and undoped KNN the relative density was around 88 %.

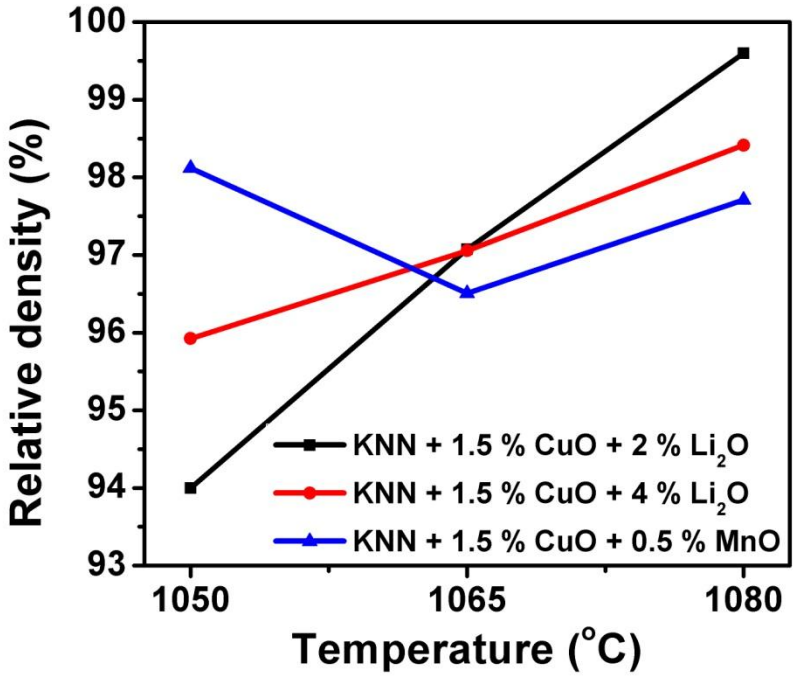

Figure 30 - Relative densities of textured doped KNN for different sintering temperatures.

Figure 31 presents the SEM micrographs of the textured doped KNN ceramics. For comparison all the micrographs have the same magnification. Ceramics are dense in agreement with the measured density and all the compositions present a clear bimodal grain size distribution: quite big grains immersed in a matrix of smaller ones. Copper manganese doped composition presents the biggest grains. The grain size distribution (Figure 32) shows an increase of large grains with the increase of the sintering temperature. The large grains grow at expenses of the small ones from the matrix due to the difference of surface free energy. The composition with the largest grains (≈80 μm of equivalent diameter) is the one with copper and manganese for the sintering temperatures ≥1065 ºC. As previously observed, for the compositions doped with copper and lithium the increase of lithium increases the grain size.

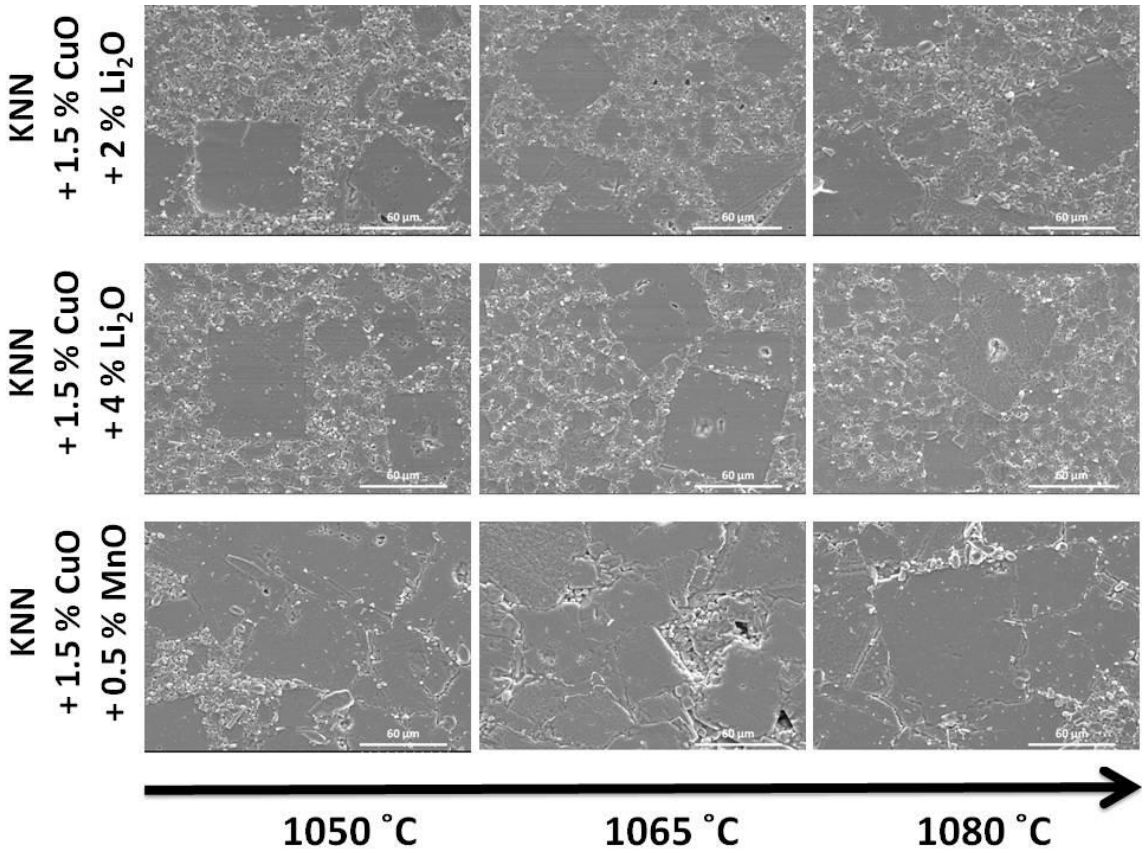

Figure 31 - SEM micrographs of textured doped KNN sintered at different temperatures.

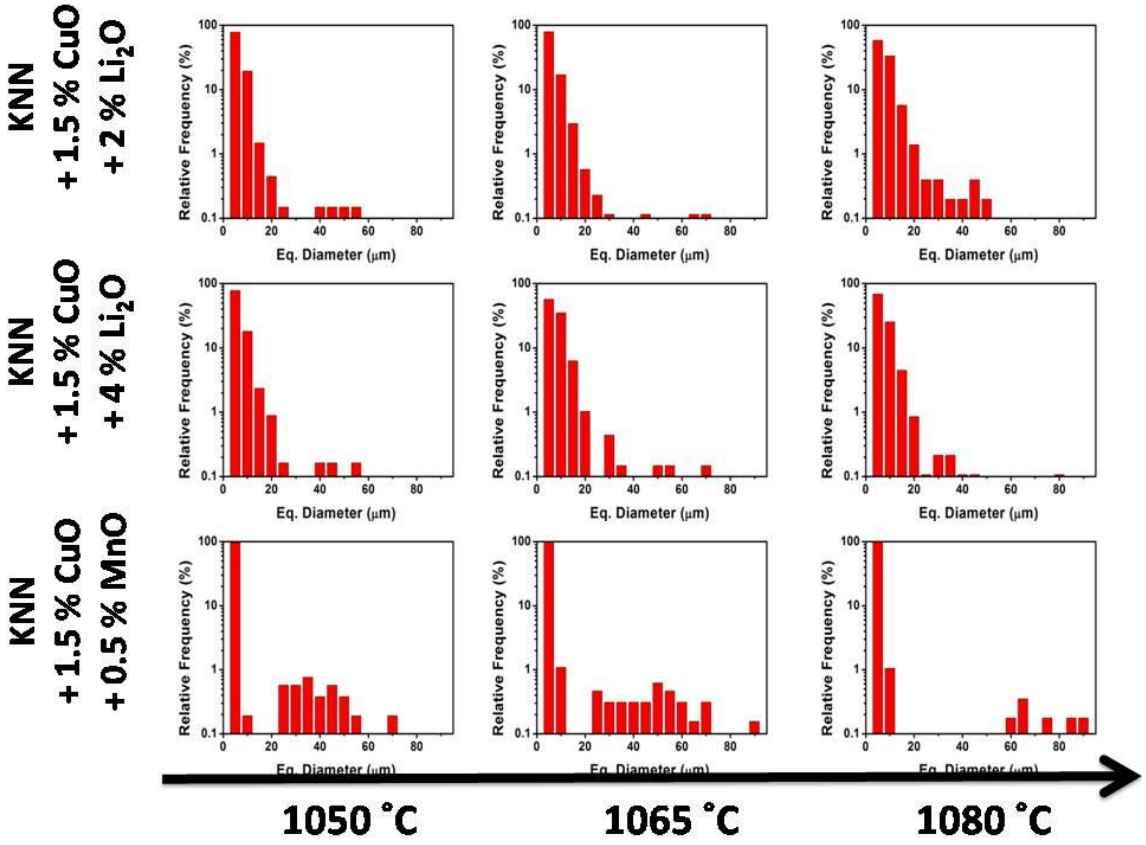

Figure 32 - Grain size distribution of textured samples of doped KNN for different temperatures.

Temperature dependence of the relative permittivity is shown in Figure 33 measured at a frequency of 1 kHz. All the textured and doped KNN ceramics showed two phase transition temperature that correspond to the monoclinic/orthorhombic to tetragonal ($T_{O\text{-}T}$) and tetragonal to cubic ($T_{T\text{-}C}$). The $T_{O\text{-}T}$ transition temperature for undoped untextured KNN ceramics was found to be 200 °C, while T_C was 420 °C, which are close to the reported values in the literature [1, 15]. The addition of dopants shifts the Curie transition to lower temperatures. The values of T_C and room temperature relative permittivity are summarized in Table 4. It can be observed that the increase of lithium increases the value of ε_r and the copper and manganese doped KNN exhibit the lowest value of ε_r at room temperature. The $T_{O\text{-}T}$ transition temperature of textured and doped KNN is lower than the untextured and undoped KNN.

Figure 34 presents the dielectric losses measured at a frequency of 1 kHz. At high temperatures the compositions doped with copper and lithium show lower losses, however the increase of amount of lithium leads to an increase of losses. Also, the composition doped with copper and manganese presents higher losses. In this case the

increase of the losses can be related with the ionic conductivity of oxygen vacancies. The doping with lower valence dopants has direct effect on the concentration of this type of defects due to the equilibrium described in Equation 7 and Equation 8.

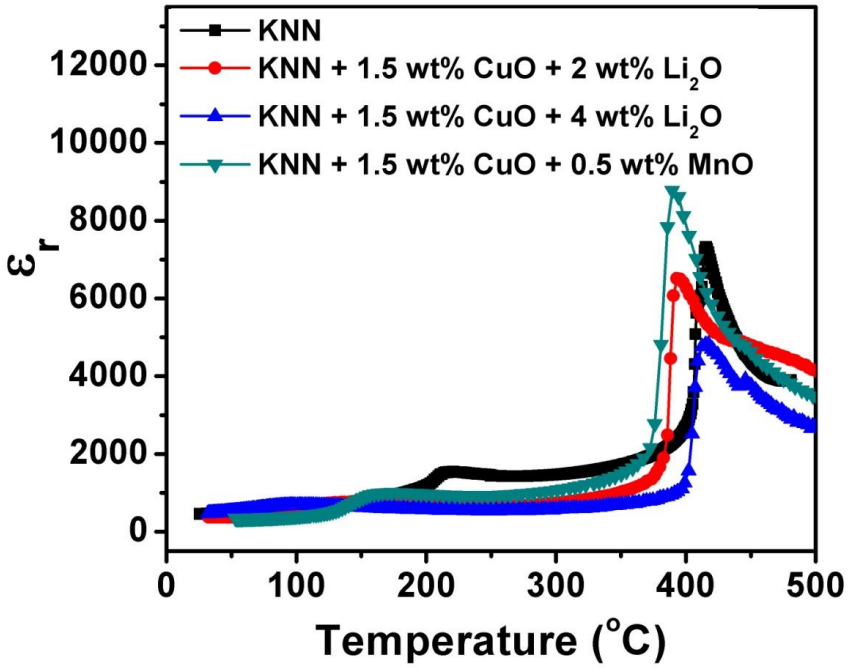

Figure 33 - Relative permittivity as a function of temperature for 1kHz of textured doped and untextured undoped KNN ceramics sintered at 1065 ˚C for 2 h.

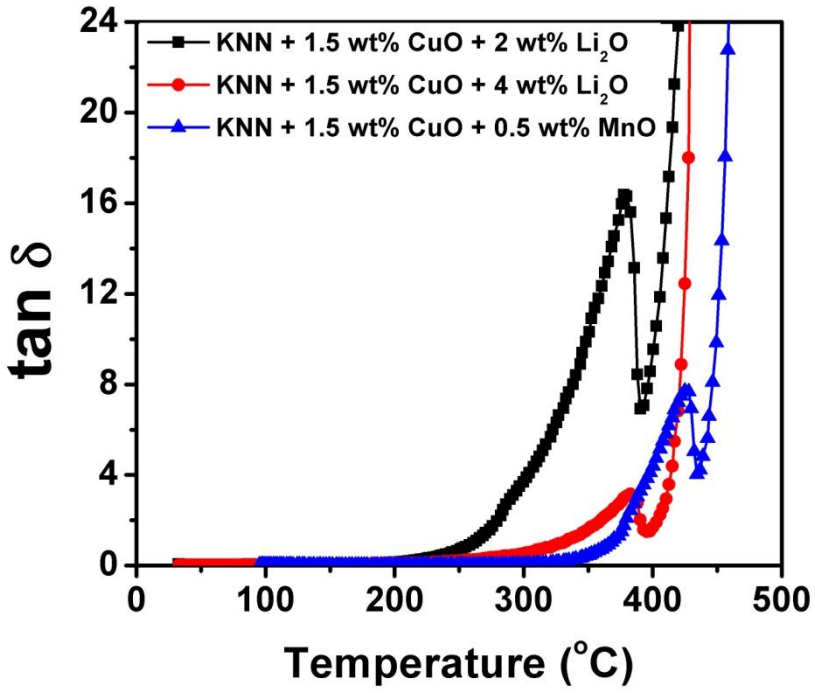

Figure 34 - Dielectric losses as a function of temperature for 1kHz of textured doped and untextured undoped KNN ceramics sintered at 1065 ˚C for 2 h.

Table 4 - Curie temperature and relative permittivity for untextured undoped and textured doped KNN samples sintered at 1065 ˚C for 2 h.

	KNN	*KNN + 1.5 mol% CuO + 2 mol% Li_2O*	*KNN + 1.5 mol% CuO + 4 mol% Li_2O*	*KNN + 1.5 mol% CuO + 0.5 mol% MnO*
Curie temperature (˚C)	**415**	**396**	**417**	**390**
ε_r	**458**	**373**	**470**	**341**

Discussion

One of the biggest problems of undoped KNN is its poor densification. Within this context, copper, lithium and manganese oxides have been reported as sintering aids for KNN densification due to the liquid phase formation [1, 15, 24].

As clearly seen from the dilatometry curves (Figure 19) an increased in the shrinkage is visible in all the doped compositions accompanied by a decrease of the onset temperature for shrinkage. Also, the density of all the compositions for untextured and textured samples was improved as can be seen in Figure 23 and 30, reaching values above 94 %. This can be attributed to the presence of the sintering aids and liquid phase formation.

Mgbemere *et al* [15] reported that for 2 % and 4 % of lithium oxide and temperatures up to 1100 ˚C there is an improvement of the density values due to the formation of extra phases. However for temperatures above 1100 ˚C the density decreases due to the high vapor pressure of alkali elements. The presence of lithium as a dopant also affcets the transitions temperatures. Li *et al* [25] showed that doping KNN with lithium has a significant impact on both transitions temperatures, lowing the orthorhombic-tetragonal transition and raising the Curie temperature. From Table 4 it can be observed that the Curie temperature for KNN doped with 1.5 mol% of CuO and 2.0 mol% of Li_2O the Curie temperature decreases. This can be related with the combined use of CuO and its effect on transition temperatures.

Alkoy *et al* [1] reported that doping KNN with CuO increases the density and grain growth with increasing amount of CuO. The authors related this observation with liquid phase formation. Liquid phase contributes to the sintering process by accelerating particle redistribution due to enhanced atomic mobility and improves final densification by capillary forces.

Also Rubio-Marcos *et al.* [24] demonstrated that the use of manganese oxide as dopant improves the density of KNN system due to liquid phase formation. The authors explained that liquid phase formation contributes to sintering by accelerating particle redistribution owing to enhanced atomic mobility. It was also reported that the presence of manganese oxide promotes the exaggerated grain growth of KNN by the difference in surface free energies between the large grains and the fine matrix, as it was seen in SEM

micrographs presented in Figure 31 of our work. This effect was also reported for copper oxide doped KNN ceramics.

As discussed before, Mn and Cu occupy B site instead of A site occupancy in perovskite structure, leading to a B site charge excess. The mechanism that is most likely to compensate for this is the formation of oxygen vacancies similar to Equation 7 and Equation 8. Kizaki *et al.* [19] reported that doped KNN results with Mn^{2+} at B site based of the fact that the lattice parameters of single crystals of KNN increase with the increasing of Mn^{2+} concentration. It is expected that in the compositions studied in this work display the same behavior and the Mn ions occupy B site positions. The same mechanism is expected for Cu doping, regular to Equation 7. Due to this a hard piezoelectric is expected [7].

From grain size distribution present in Figure 25,Figure 25 it can be seen that copper and lithium oxide as a dopant affect more the grain size growth. Furthermore, it can be seen that the grain growth increases with the increasing of lithium oxide. This can occur due to the increased content of liquid phase in copper and lithium oxide doped KNN comparing with copper and manganese oxide doped KNN. However, when we observe the grain size distribution in textured samples (Figure 32) copper and manganese oxides promote grain growth of large grains. Comparing with copper and lithium oxide compositions, doping with copper and manganese enhances the effect of abnormal grain growth. On the other hand, volatility effects from A site cations are quite common. The volatilization of A-site cations creates A vacancies and holes according to equation (in Kroger-Vink notation):

$$A_A \rightarrow V_A'' + 2h^{\cdot} \qquad \text{Equation 12}$$

where A_A is an A site ion in network position A, $V_{A''}$ is a A site vacancy and $h^{\cdot}$ is a electron hole. Doping with Li_2O provides monovalent cations capable of occupying this A-site vacancies. Note that the increase of Li_2O leads to larger grain size distribution. In case of KNN doped with CuO and MnO, there is no occupation of A-site vacancies.

The above presented results allow to conclude that all the compositions led to dense ceramics. The sintering temperature should be a minimum of 1065 ˚C to ensure single phase system.

From the X-ray diffraction patterns present in Figure 20, 21, 22, 26, 27 and 28, it can be observed that KNN compositions with copper and lithium sintered at temperatures below 1065 ˚C present secondary phases. This does not happen for copper and manganese oxides doped KNN ones. Due to this, can be concluded that compositions doped with copper and manganese are more stable. In addition and based on the Lotgering factors (Figure 29), compositions with copper and manganese oxide present the best values of texturization reaching ≈19 %. It is expected that this composition exhibits high values of piezoelectric coefficient. For these reasons, the composition doped with copper and manganese and the temperature of 1065 ˚C were chosen for the second part of this work.

Part II

Abstract

Based on the previous results, in this part of work KNN + 1.5 mol% CuO + 0.5 mol% MnO composition was selected to improve the texturization of these ceramics. Hence for a sintering temperature of 1065 ˚C the effect of the amount of single crystals added as templates, of the heating rate during sintering and dwell time at the maximum sintering temperature was studied in the texturization. The amount of single crystals used varried from 2.5 wt%, 5.0 wt% and 10 wt% of single crystals for a sintering rate of 10 ºC/min for 24 hours. In order to study the effect of the heating rate, compositions with 5.0 wt% of single crystals were sintered for 24 hours at 1065 ˚C with the heating rates of 2 ºC/min, 10 ºC/min and 20 ºC/min. For the composition with 5 wt% of single crystals and heated at 10 ºC/min, dwell time was 4, 16 and 24 h.

Phase purity

X-ray diffraction patterns of all samples are displayed in Figure 35Figure 35, 36 and 37. All of the samples show monophasic KNN.

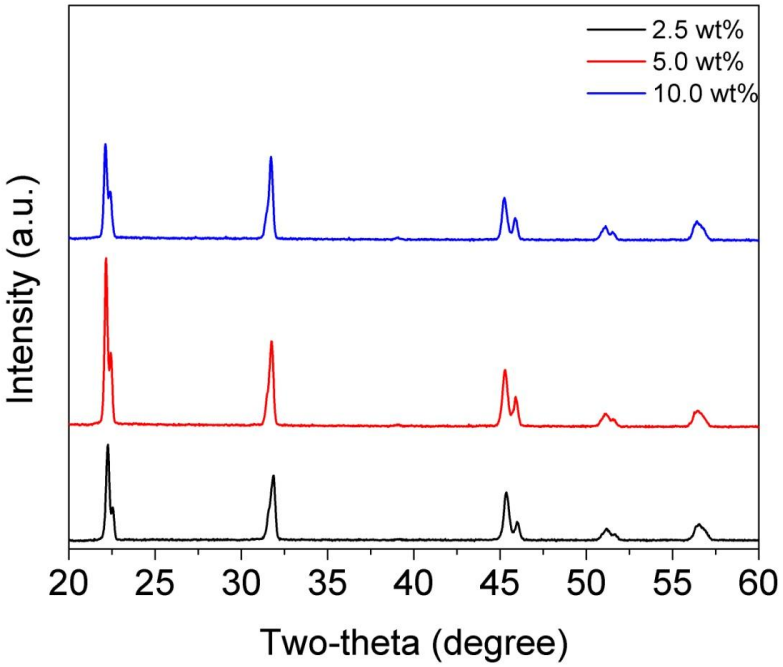

Figure 35 - X-ray diffraction patterns of the samples of KNN+1.5% CuO+0.5% MnO sintered at 1065 ˚C for 24 hours, ranging the amount of single crystals.

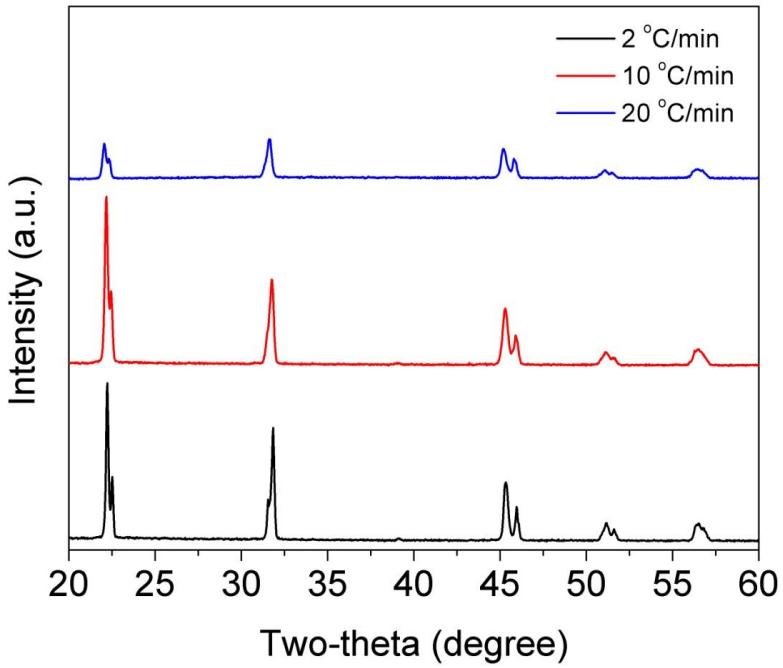

Figure 36 - X-ray diffraction patterns of the samples of KNN+1.5% CuO+0.5% MnO sintered at 1065 ˚C for 24 hours, with 5 wt% of single crystals, ranging the heating/cooling rate.

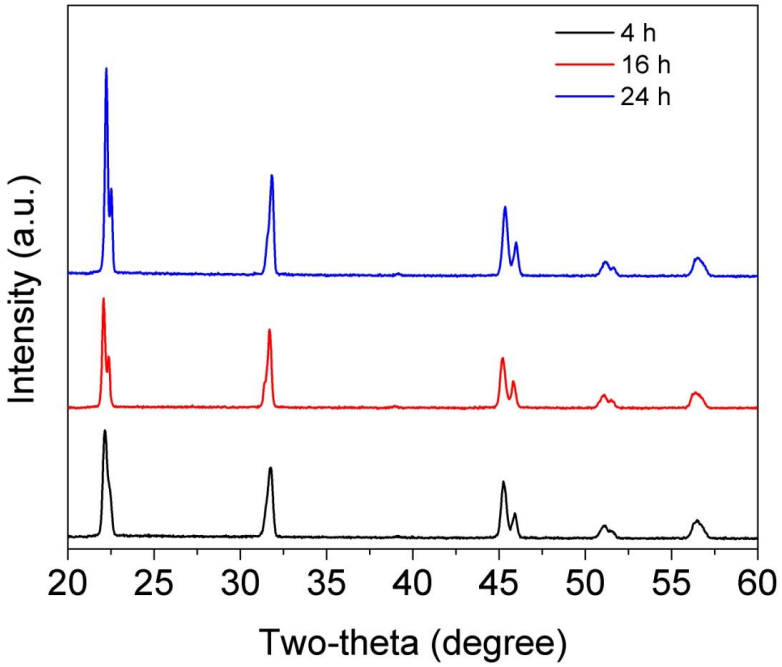

Figure 37 - X-ray diffraction patterns of the samples of KNN+1.5% CuO+0.5% MnO sintered at 1065 ˚C with 5 % of single crystals and an heating ratio of 10 ˚C/min, ranging the dwelling time.

Degree of texture

The calculated Lotgering factors are given in Table 5. The Lotgering factor varied from 28.6 % to 37.8 % wherein the best result is for KNN+1.5% CuO+0.5% MnO with 5 wt% of single crystals, sintered for 24 h with 10 ˚C/min of heating rate.

Microstructure and density of sintered samples

The density of textured KNN + 1.5 mol% CuO + 0.5 mol% MnO ceramics is shown in Table 6 as percentage of theoretical density (4.51 g/cm^3). As previously observed, all sintered ceramics reached more than 95 % of theoretical density, with the highest density obtained being 99.8 % for the sample with 5 wt% of single crystals, 2 ˚C/min and 24 h of dwell time.

Figure 38, 39 and 40 illustrate the micrographs of textured KNN + 1.5 mol% CuO + 0.5 mol% MnO ceramics. For comparison purposes all the micrographs have the same magnification.

Table 5 - Calculated Lotgering factors for textured KNN+1.5% CuO+0.5% MnO ceramics.

	Conditions		*Lotgering factor (%)*
% of single crystals	**2.5**		**28.8**
	5.0	**10 ˚C/min, 24 h**	**37.8**
	10.0		**29.6**
Heating rate (˚C/min)	**2**		**29.9**
	10	**5 % of single crystals, 24 h**	**37.8**
	20		**28.6**
Dwelling time (h)	**4**		**30.7**
	16	**5 % of single crystals, 10 ˚C/min**	**36.6**
	24		**37.8**

Table 6 - The density of textured KNN + 1.5 mol% CuO + 0.5 mol% MnO ceramics sintered under different conditions.

	Conditions		Relative density (%)
% of single crystals	**2.5**	**10 ˚C/min, 24 h**	**96.3**
	5.0		**95.8**
	10.0		**96.6**
Heating rate (˚C/min)	**2**	**5 % of single crystals, 24 h**	**99.8**
	10		**95.8**
	20		**95.9**
Dwelling time (h)	**4**	**5 % of single crystals, 10 ˚C/min**	**95.3**
	16		**98.4**
	24		**95.8**

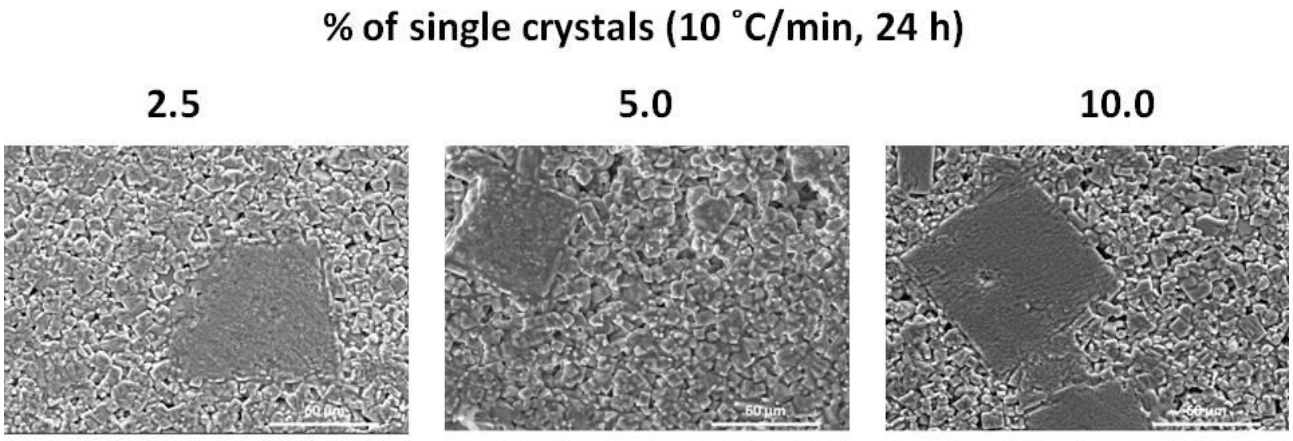

Figure 38 - SEM micrographs of textured KNN + 1.5 mol% CuO + 0.5 mol% MnO sintered with 10 ˚C/min for 24 h at 1065 ˚C, ranging the amount of single crystals.

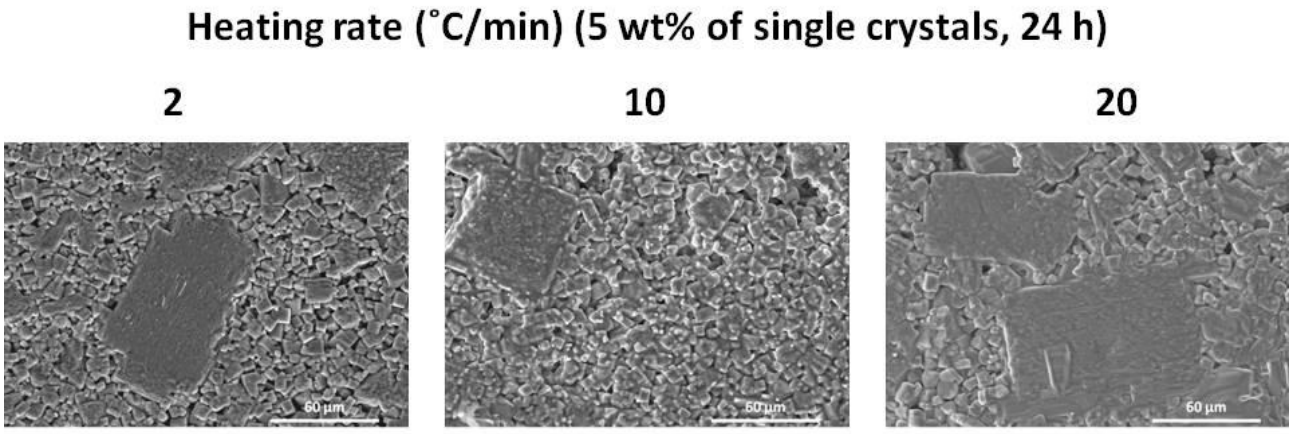

Figure 39 - SEM micrographs of textured KNN + 1.5 mol% CuO + 0.5 mol% MnO with 5 wt% of single crystals, sintered for 24 h at 1065 ˚C, ranging the heating rate.

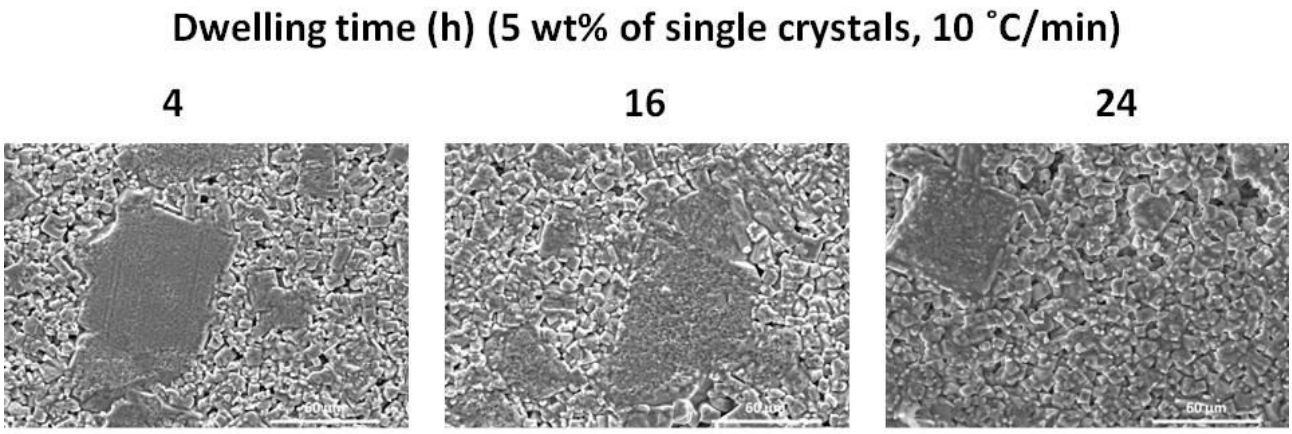

Figure 40 - SEM micrographs of textured KNN + 1.5 mol% CuO + 0.5 mol% MnO with 5 wt% of single crystals, sintered with 10 ˚C/min at 1065 ˚C, ranging the dwelling time.

Dielectric properties

Plots of relative permittivity and dielectric loss versus temperature for KNN + 1.5 mol% CuO + 0.5 mol% MnO are shown in Figure 41 and 42, respectively. For comparison, relative permittivity of pure KNN is presented as well. Both samples were measured on cooling from 500 ˚C to room temperature at 2 ˚C/min for 1 kHz. The KNN ceramics are hygroscopic, due to that the dielectric curves presented are from the cooling in order to

avoid the contribution of superficial conduction. A magnification of orthorhombic to tetragonal transition, T_{O-T}, area is presented in Figure 43. It can be seen that for pure KNN the transition temperature is around 210 ˚C, but, for the composition studied in this part the transition occurs at lower temperature (≈170 ºC) and it is smooth.

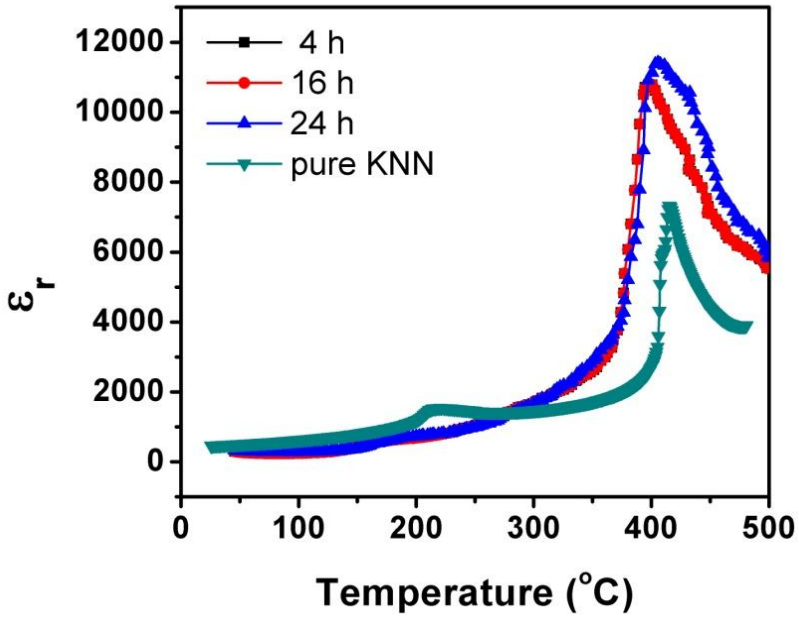

Figure 41 - Relative permittivity (at 1 kHz) of KNN + 1.5 mol% CuO + 0.5 mol% MnO with 5 wt% of KNN single crystals and sintered at 1065 ˚C with an heating ratio of 10 ˚C/min for different dwell times.

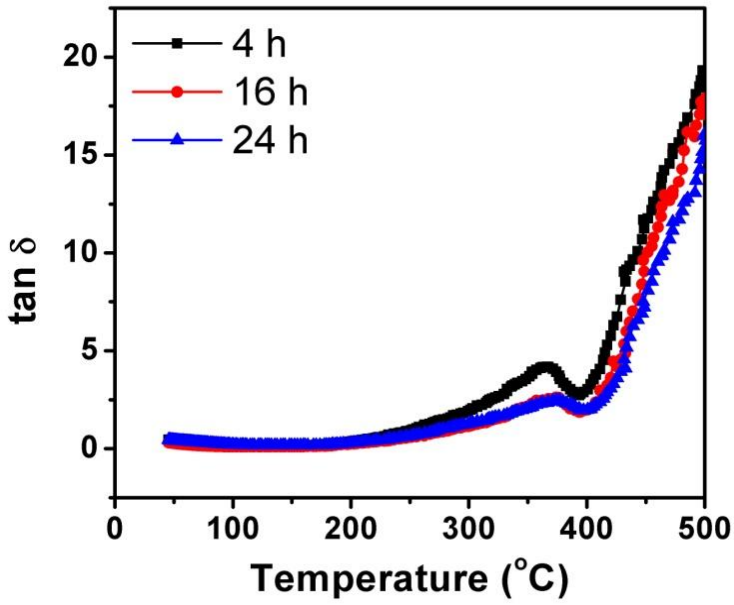

Figure 42 - Dielectric losses (at 1 kHz) of KNN + 1.5 mol% CuO + 0.5 mol% MnO with 5 wt% of KNN single crystals and sintered at 1065 ˚C with an heating ratio of 10 ˚C/min for different dwell times.

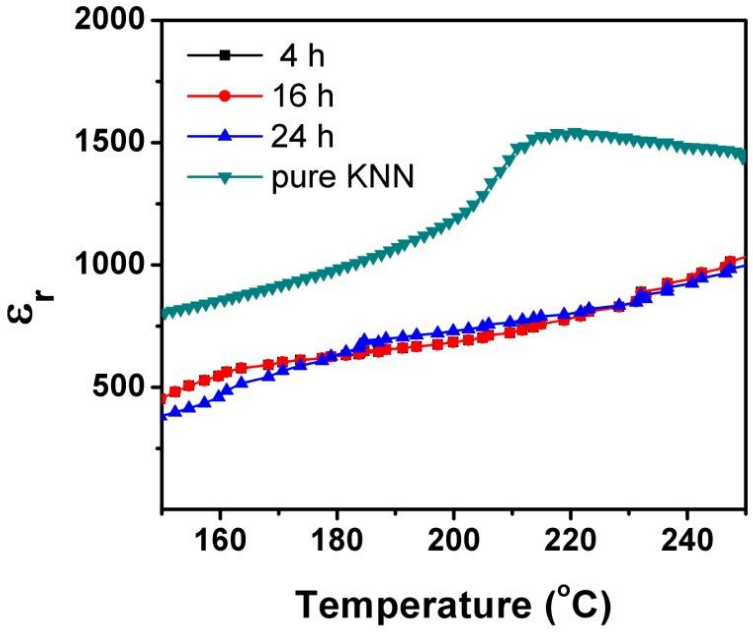

Figure 43 - Magnification of area around O-T transition of KNN + 1.5 mol% CuO + 0.5 mol% MnO with 5% of single crystals sintered at 1065 ˚C for 4, 16 and 24 h with 10 ˚C/min of heating rate and pure KNN sintered at 1100 ˚C for 4 h.

Relative permittivity and dielectric loss versus temperature at different frequencies are given in Figure 44 and 45, respectively. Both were measured on cooling from 500 ˚C to room temperature at 2 ˚C/min, for frequencies ranging from 100 Hz to 1 MHz.

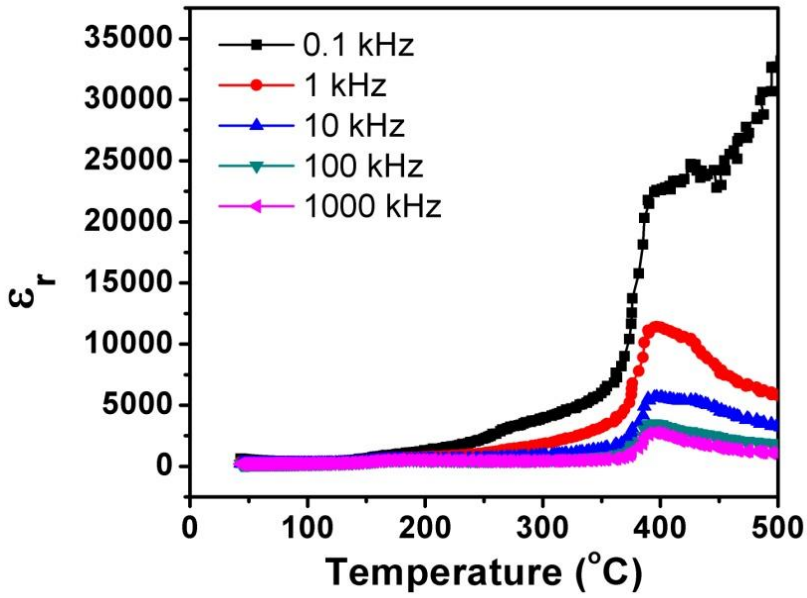

Figure 44 - Dielectric permittivity of KNN + 1.5 mol% CuO + 0.5 mol% MnO with 5% of single crystals sintered at 1065 ˚C for 24 h with 10 ˚C/min of heating rate as function of temperature for different frequencies.

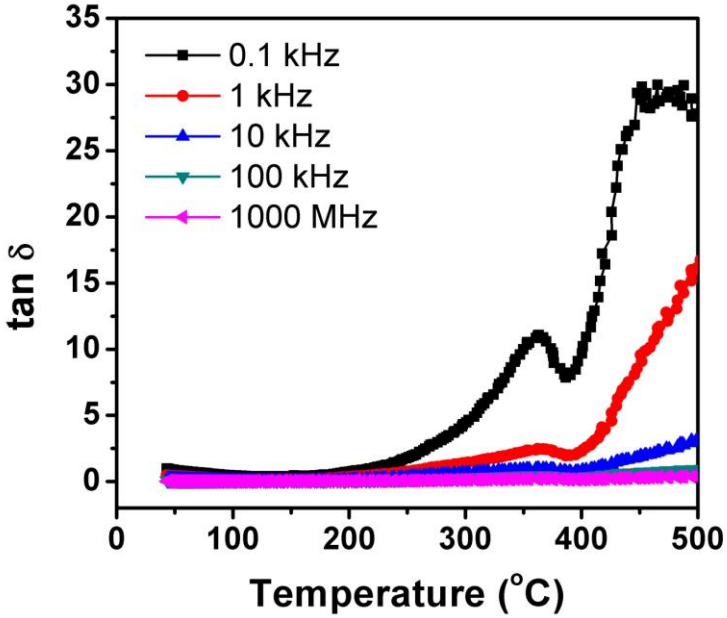

Figure 45 - Dielectric losses of KNN + 1.5 mol% CuO + 0.5 mol% MnO with 5% of single crystals sintered at 1065 ˚C for 24 h with 10 ˚C/min of heating rate as function of temperature for different frequencies.

Piezoelectric properties

Figure 46 and 47 present the piezoelectric coefficient (d_{33}) and piezoelectric voltage constant (g_{33}) as function of the Lotgering factor, respectively. As expected the piezoelectric coefficient increases with the increase of the Lotgering factor what might be related with the increase of polarization and alignment of the ferroelectric domains as grains growth along the single crystal polarization direction. The maximum d_{33}belong to the sample with 5 wt% of single crystals sintered at 1065 ºC for 24 h with a heating / cooling rate of 10 ºC/min. Note that the piezoelectric coefficient increases with increasing Lotgering factor. However, the achieved piezoelectric voltage constant is maximum for 36 % of Lotgering factor. The piezoelectric voltage coefficient is dependent on the piezoelectric coefficient and relative permittivity and the preferential crystallographic orientation has effect in both in different ways. Due to this, there is a commitment between the impact of texturization on piezoelectric coefficient and piezoelectric voltage constant.

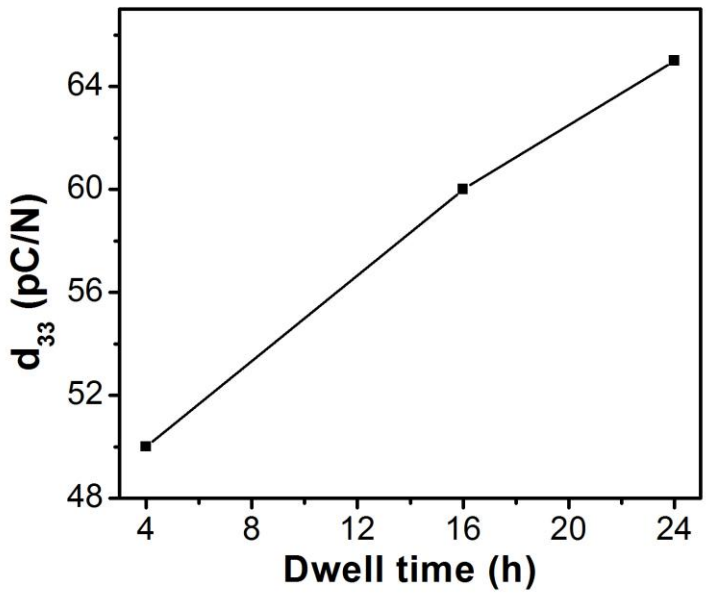

Figure 46 - Piezoelectric coefficient versus dwell time of KNN + 1.5 mol% CuO + 0.5 mol% MnO with 5% of single crystals sintered at 1065 ˚C with 10 ˚C/min of heating rate.

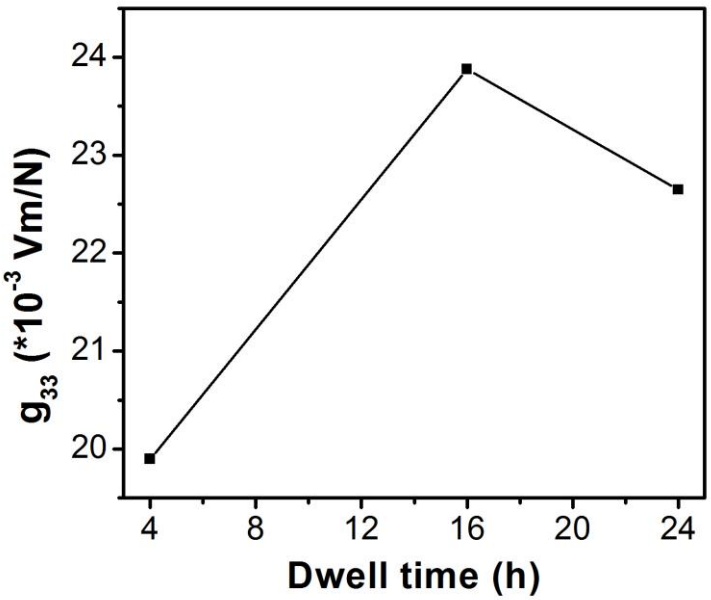

Figure 47 - Piezoelectric voltage constant versus dwell time of KNN + 1.5 mol% CuO + 0.5 mol% MnO with 5% of single crystals sintered at 1065 ˚C with 10 ˚C/min of heating rate.

Discussion

In this part of the work all of the samples exhibit monophasic compositions. Also in terms of the preferential orientation, evaluated by Lotgering factor, it was possible to increase its degree by optimization of the processing conditions (the amount of single crystals and the heating rate) and the values were improved from ≈19 % to 38 %.

The calculated Lotgering factor is given in Table 5. The Lotgering factor varied from 28.6 % to 37.8 % wherein the best results is for KNN + 1.5 % CuO + 0.5 % MnO with 5 wt% of single crystals, sintered for 24 h with 10 ºC/min of heating.

Table 6 shows that all of the ceramics were dense, proving the effective role of the dopants in KNN ceramics. It can be seen that the increasing of heating rate causes a decrease of density (Table 7). It was expected that in dwell time ranging, the larger grains growth at expense of all of small grains. However, it can be seen that there is no significant difference between 4 and 24 hours. This can occur due to the remain porosity; small pores around the larger grains are observed. These pores stopped the grain growth, working like a barrier to continuous growth of the larger grains.

It can be seen that the transition from monoclinic to tetragonal is very smooth and not visible (Figure 41 and 43). This can be related to the presence of oxygen vacancies as discussed in Part I. Oxygen vacancies may reduce the distortion of the unit cell as suggested by Kang *et al.* [11], based on the study of the effect of atmosphere during KNN sintering. It was also reported that reducing atmosphere may cause the shift of monoclinic-tetragonal transition temperature to lower temperatures. It is possible that the added dopants promote the formation of oxygen vacancies and produce a similar effect to the one observed for reducing atmosphere. It is also possible that oxygen vacancies induced by the added dopants affect negatively the piezoelectric properties of KNN. For further considerations a sintering study with different atmospheres and the role of copper and manganese oxides in terms of unit cell distortion and its effect on piezoelectric properties needs to be conducted.

Table 7 - Properties of KNN + 1.5 mol% CuO + 0.5 mol% MnO with 5% of single crystals sintered at 1065 ˚C with 10 ˚C/min of heating rate, ranging the dwelling time (4, 16 and 24 h).

Time (h)	Relative density (%)	Lotgering factor (%)	T_C (˚C)	d_{33} (pC/N)	g_{33} (*10^{-3} Vm/N)
4	95.3	30.7	400.8	50	19.9
16	98.4	36.6	402.9	60	23.9
24	95.8	37.7	396.9	65	22.6

On the other hand, it is possible to observe that preferential orientation has a real effect in piezoelectric coefficient (Figure 46). It is expected that higher Lotgering factor leads to higher piezoelectric coefficient. However, using pressing as a conformation step to achieve preferential orientation higher than 40 % seems to be very difficult.

From the application point of view, actuators require large piezoelectric coefficients; however, sensors require a small piezoelectric coefficient. Hence sensors are usually evaluated in terms of piezoelectric voltage constant while one of the requirements for actuators is a high piezoelectric coefficient.

Comparing the properties with commercial PZTs, the KNN produced in this work can be useful and a viable alternative to PZT for sensor devices. Indeed the piezoelectric voltage constant of textured KNN + 1.5 mol% CuO + 0.5 mol% MnO ceramics is in the range of PZT and in some cases higher (see Table 8).

An interesting fact is that the KNN produced in this work keep the high Curie temperature (400 ºC) allowing application at high temperatures. This was one of the main objectives in this work.

In order to improve the electromechanical response of this particular composition, a study of the sintering atmospheres is needed. In addition to obtain higher Lotgering factors, different processing techniques need to be taken into account like tape casting.

Table 8 - Comparison between properties of commercial PZT and KNN + 1.5 mol% CuO + 0.5 mol% MnO with 5% of single crystals sintered at 1065 ˚C with 10 ˚C/min of heating rate, dwelling time (16h).

Composition	g_{33} (*10^{-3} Vm/N)	d_{33} (pC/N)	ε_r	T_C (ºC)	Ref.
PZT Navy Type I	24.6	290	1435	320	[26]
PZT Navy Type II	25.2	400	1770	365	[26]
PZT Navy Type V	22.6	530	2650	>250	[26]
PZT 3195STD	24.2	350	1800	350	[27]
PZT 3203STD	19.0	550	3250	235	[27]
KNN in this work	23.9	60	300	≈400	

Conclusions

The main conclusions of this thesis work can be summarized as follows:

- Doping KNN with i) 1.5 mol% CuO and 2 mol% Li_2O, ii) 1.5 mol% CuO and 4 mol% Li_2O, and iii) 1.5 mol% CuO and 0.5 mol% MnO, allowed to obtain dense ceramics (densification >94 %).
- Copper and manganese proved to be the dopant combination that promotes most abnormal grain growth, resulting in higher Lotgering factor, hence in the enhancement of the piezoelectric properties.
- The best Lotgering factors (≈ 38%) were obtained for the composition KNN + 1.5 mol% CuO + 0.5 mol% MnO, plus 5 wt% of single crystals, sintered at 1065 ºC for 24 h and 16 h and 10 ºC/min of heating/cooling rate with a d_{33} of 65 pC/N and g_{33} of 23,9 Vm/N, respectively.
- This piezoelectric voltage constant (g_{33} of 23,9 Vm/N) is comparable to that of commercial PZT, but keeping a high Curie temperature (400 ºC).

References

1. Alkoy, E.M., et al., *Microstructural features and electrical properties of copper oxide added potassium sodium niobate ceramics.* Ceramics International, 2010. **36**(6): p. 1921-1927.
2. López-Juárez, R., et al., *Ferroelectric domain structure of lead-free potassium-sodium niobate ceramics.* Journal of the European Ceramic Society, 2011. **31**(9): p. 1861-1864.
3. *Directive 2002/95/EC of the European Parliament and of the Council on the restriction of the use of certain hazardous substances in electrical and electronic equipment.* Official Journal of the European Union, 2003.
4. Saito, Y., et al., *Lead-free piezoceramics.* Nature, 2004. **432**(7013): p. 84-87.
5. A/S, F.P., *Stakeholder consultation on Adaptation to scientifica and technical progress under Directive 2002/95/EC (RoHS) of the European Parliament and of the Council for the porpuse of a possible amendment of the Annex.* 2008.
6. chemPUR. *http://chempur.de/index.php?index=1&lng=en&menuid=25*. 2014 [cited 2014 June 10th].
7. Bernard Jaffe, et al., *Piezoelectric ceramics*. Non-Metallic Solids, Vol. 3. 1971: Academic Press. 317.
8. Haertling, G.H., *Ferroelectric ceramics: History and technology.* Journal of the American Ceramic Society, 1999. **82**(4): p. 797-818.
9. Patel, I., *Ceramic Based Intelligent Piezoelectric Energy Harvesting Device*. Advances in Ceramics - Electric and Magnetic Ceramics, Bioceramics, Ceramics and Environment, ed. P.C. Sikalidis. 2011.
10. *https://www.americanpiezo.com/knowledge-center/piezo-theory/piezoelectric-constants.html*. [cited 2014 October].
11. Fisher, J.G., et al., *Structural changes in potassium sodium niobate ceramics sintered in different atmospheres.* Journal of Alloys and Compounds, 2009. **479**(1–2): p. 467-472.
12. Rafiq, M.A., et al., *Establishing the Domain Structure of $(K_{0.5}Na_{0.5})NbO_3$ (KNN) Single Crystals by Piezoforce-Response Microscopy*. Science of Advanced Materials, 2014. **6**(3): p. 426-433.

13. Shrout, T.R. et al., *Lead-free piezoelectric ceramics: Alternatives for PZT?* Journal of Electroceramics, 2007. **19**(1): p. 113-126.
14. Rodel, J., et al., *Perspective on the Development of Lead-free Piezoceramics.* Journal of the American Ceramic Society, 2009. **92**(6): p. 1153-1177.
15. Mgbemere, H.E., et al., *Investigation of the dielectric and piezoelectric properties of potassium sodium niobate ceramics close to the phase boundary at $(K_{0.35}Na_{0.65})NbO_3$ and partial substitutions with lithium and antimony.* Journal of the European Ceramic Society, 2009. **29**(15): p. 3271-3276.
16. Mgbemere, H.E., et al., *Effect of MnO_2 on the dielectric and piezoelectric properties of alkaline niobate based lead free piezoelectric ceramics.* Journal of the European Ceramic Society, 2009. **29**(9): p. 1729-1733.
17. Tkach, A., et al., *Structure-microstructure-dielectric tunability relationship in Mn-doped strontium titanate ceramics.* Acta Materialia, 2005. **53**(19): p. 5061-5069.
18. Matsumoto, K., et al., *Electric-field-induced strain in Mn-doped $KNbO_3$ ferroelectric ceramics.* Ceramics International, 2008. **34**(4): p. 787-791.
19. Kizaki, Y., et al., *Defect control for low leakage current in $K_{0.5}Na_{0.5}NbO_3$ single crystals.* Applied Physics Letters, 2006. **89**(14).
20. Messing, G.L., et al., *Templated grain growth of textured piezoelectric ceramics.* Critical Reviews in Solid State and Materials Sciences, 2004. **29**(2): p. 45-96.
21. *Image Processing and Analisys in Java*. [cited 2014 Jan]; Available from: http://imagej.nih.gov/ij/.
22. Buchanan, R.C., *Ceramic materials for electronics*. 3rd ed. 2004: Marcel Dekker Inc.
23. Huang, Z., et al., *Determination of piezoelectric coefficients and elastic constant of thin films by laser scanning vibrometry techniques.* Sensors and Actuators a-Physical, 2007. **135**(2): p. 660-665.
24. Rubio-Marcos, F., et al., *Effect of MnO doping on the structure, microstructure and electrical properties of the $(K,Na,Li)(Nb,Ta,Sb)O_3$ lead-free piezoceramics.* Journal of Alloys and Compounds, 2011. **509**(35): p. 8804-8811.
25. Li, J.F., et al., *$(K, Na) NbO_3$-Based Lead-Free Piezoceramics: Fundamental Aspects, Processing Technologies, and Remaining Challenges.* Journal of the American Ceramic Society, 2013. **96**(12): p. 3677-3696.

26. *http://www.morganelectroceramics.com/resources/piezo-ceramic-tutorials/typical-properties/*. [cited 2014 October].
27. *http://www.ctscorp.com/components/pzt/downloads/PZT_5Aand5H.pdf*. [cited 2014 October].